# Structural studies on members of the picornavirus superfamily

**JANI J.T. SEITSONEN**

Institute of Biotechnology
and
Department of Biosciences
Division of Genetics
Faculty of Biological and Environmental Sciences
University of Helsinki
and
National Graduate School in Informational and Structural Biology

ACADEMIC DISSERTATION

To be presented for public examination with the permission of the Faculty of Biological and Environmental Sciences of the University of Helsinki in the auditorium 1041 of Biocenter 2, Viikinkaari 5, Helsinki, on February 18th, 2011, at 12 noon

HELSINKI 2011

**Supervisor**

Professor Sarah J. Butcher
Institute of Biotechnology
University of Helsinki

**Custodian**

Professor Juha Partanen
Institute of Biotechnology
University of Helsinki

**Reviewers**

Academy professor Jari P. Valkonen
Department of Agricultural Sciences
University of Helsinki

Professor Pirkko Heikinheimo
Institute of Biotechnology
University of Helsinki

**Follow-up group**

Professor Timo Hyypiä
Department of Virology
University of Turku

Professor Pirkko Heikinheimo
Institute of Biotechnology
University of Helsinki

**Opponent**

Professor Peter G. Stockley
The Astbury Centre for Structural
Molecular Biology
University of Leeds

ISBN 978-952-10-6799-0 (paperback)
ISBN 978-952-10-6800-3 (PDF, http://ethesis.helsinki.fi/)

ISSN 1795-7079

Yliopistopaino, Helsinki University Printing House
Helsinki 2011

**To Hanna**

# Table of contents

# Original publications

This thesis is based on the following two articles and one unpublished manuscript, which are referred to in the text by their Roman numerals.

**I** Seitsonen, J.J.T., Susi, P., Lemmetty, A. and Butcher S.J. (2008) Structure of the mite-transmitted *Blackcurrant reversion nepovirus* using electron cryo-microscopy. Virology, 378(1):162-8.

**II** Seitsonen, J., Susi, P., Heikkilä, O., Sinkovits, R.S., Laurinmäki, P., Hyypiä, T. and Butcher S.J. (2010) Interaction of $\alpha_V\beta_3$ and $\alpha_V\beta_6$ Integrins with Human Parechovirus 1. J Virol. 84(17):8509-19.

**III** Seitsonen, J.J.T., Susi, P., Sinkovits, R.S., Hyvönen, H., Laurinmäki, P., Ylä-Pelto, J., Hyypiä, T. and Butcher, S.J. (Unpublished) Cryoelectron microscopy analysis of coxsackievirus A7 and structural changes associated with uncoating.

# Abbreviations

| | |
|---|---|
| BRD | Blackcurrant reversion disease |
| BRV | Blackcurrant reversion virus |
| CAV7 | Coxsackievirus A7 |
| CAV9 | Coxsackievirus A9 |
| CCD | Charge-coupled device |
| CCMV | Cowpea chlorotic mottle virus |
| CD155 | Cluster of differentiation 155 |
| CNS | Central nervous system |
| cryoET | Cryo electron tomography |
| cryoTEM | Cryo transmission electron microscopy |
| CTF | Contrast transfer function |
| EV71 | Enterovirus 71 |
| EV9 | Echovirus 9 |
| FMDV | Foot-and-mouth disease virus |
| FEG | Field emission gun |
| HEV-A | Human enterovirus group A |
| HEV-C | Human enterovirus group C |
| HIV | Human immunodeficiency virus |
| HIV1 | Human immunodeficiency virus 1 |
| HPEV1 | Human parechovirus 1 |
| HRV-B | Human rhinovirus group B |
| HRV14 | Human rhinovirus 14 |
| ICAM-1 | Intracellular adhesion molecule 1 |
| IPV | Inactivated polio vaccine |
| $LaB_6$ | Lanthanum hexaboride |
| MRI | Magnetic resonance imaging |
| MS2 | Bacteriophage MS2 |
| OPV | Oral polio vaccine |
| PSF | Point spread function |
| pT-number | Pseudo triangulation number |
| PV1 | Poliovirus 1 |
| RGD | Arginine-glycine-aspartic acid |
| RMSD | Root mean square deviation |
| RNA | Ribonucleic acid |
| ss | Single stranded |
| T-number | Triangulation number |
| TEM | Transmission electron microscope |
| TMV | Tobacco mosaic virus |
| TRSV | Tobacco ringspot virus |
| VDPV | Vaccine-derived poliovirus |
| VP | Viral protein |
| Å | Angstrom |

# ABSTRACT

The pathogenic members of the picornavirus superfamily have adverse effects on humans, their crops and their livestock. As structure is related to function, detailed structural studies on these viruses are important not only for fundamental understanding of the viral life cycle, but also for the rational design of vaccines and inhibitors for disease control. These viruses have positive sense, single-stranded RNA genomes enclosed in a protein capsid. X-ray crystallography and cryo-electron microscopy studies have revealed that the isometric members of this group have icosahedrally-symmetric capsids made up of 60 copies of each of the structural proteins. The members that infect animal cells often employ one or more cellular receptors to facilitate cell entry which in some cases is known to initiate the uncoating sequence of the genome. The nature of the interactions between individual viruses and alternative cellular receptors has rarely been probed. The capsid assembly of the members of the picornavirus superfamily is considered to be cooperative and the interactions of RNA and capsid proteins are thought to play an important role in orchestrating virus assembly.

The major aims of this thesis were to solve the structures of blackcurrant reversion virus (BRV), human parechovirus 1 (HPEV1) and coxsackievirus A7 (CAV7), as well as the structure of HPEV1 complexed with two of its cellular receptors using cryo-electron microscopy, three-dimensional image reconstruction and homology modeling. Each of the selected viruses represents a taxonomic group where little or no structural data was previously available. The results enabled the detailed comparison of the new structures to those of known picornaviruses, the identification of surface-exposed epitopes potentially important for host interaction, the mapping of RNA-capsid protein interactions and the elucidation of the basis for the specificity of two different receptor molecules for the same capsid. This work will form the basis for further studies on the influence of RNA on parechovirus assembly as a potential target for drug design.

# A. INTRODUCTION

Viruses are peculiar organisms; they have no metabolism of their own and thus they are dependent on the metabolism of their host cell for reproduction. Despite their dependence on other organisms, viruses manage to exist in great numbers and are perhaps the most numerous organisms on Earth (Bamford et al., 2005; Wommack and Colwell, 2000). Viruses are known to infect cells in all branches of life, and interestingly viruses that have a parasitic relationship with a larger virus have been discovered (Briani et al., 2001; Brown, 2010; Desnues and Raoult, 2010).

To gain access to the resources of a host cell the virus must first insert, at least, the viral genome in the cytoplasm of the cell. In animal cells the entry often involves exploitation of the cells' own intake mechanisms, such as endocytosis (Mercer et al., 2010). Alternatively, many enveloped viruses, such as human immunodeficiency virus (HIV), are able to fuse their enveloping membrane with the cellular membrane of the host, allowing insertion of the viral capsid in the cytoplasm of the host cell (Tilton and Doms, 2010). In plants, viruses rely on the help of larger organisms to either deliver them directly inside the plant or at least to an opening from where entry may proceed (Brault et al., 2010; Shaw, 1999; Wang et al., 2002).

Even though viral infections in humans are often treatable, viruses are annually responsible for numerous deaths worldwide. Rotavirus alone has been estimated to be responsible for 527000 deaths annually among children under five years of age, which equals 29 % of the deaths due to diarrhea (Parashar et al., 2009). In addition to immediately fatal infections a great number of persistent viral infections occur each year. For example, in 2007 around 33 million people were estimated to live with HIV and 127 million with hepatitis C (De Cock and De Lay, 2008; Dehesa-Violante and Nunez-Nateras, 2007). The persistent infections may eventually lead to death, even with proper medical care. However, some struggles against viruses have been successful, of which the best example for picornaviruses is the eradication of poliovirus. Due to a massive vaccination campaign organized in 1988 by the World Health Organization, Rotary International, the US Centers for Disease Control and Prevention, and UNICEF, polio has become an extremely rare disease nowadays (Robbins and de Quadros, 1997).

In plants, viruses cause significant economic losses annually and often the damage caused to

crops by viruses outweighs the damage caused by their vectors (Dedryver et al., 2010). As plant viruses require the help of a vector for transmission, chemicals have been used to protect the crops from the vectors. However, chemical control is not effective in guarding against all viral infections (Perring et al., 1999; Reddy et al., 2009). To enhance the resistance of plants against viral infections, genetically engineered plants with viral RNA silencing abilities have been engineered (Collinge et al., 2010; Reddy et al., 2009; Wu et al., 2010). Many plant viruses have also yielded efficient tools for studying plant gene function (Macfarlane, 2010; Purkayastha and Dasgupta, 2009). While plant viruses pose no direct threat to human beings, they can cause severe losses in the yield of food crops, which is potentially disastrous to a small, isolated society relying on their own agricultural products.

The picornavirus superfamily is a large group of viruses that contains picorna-, como-, nepo-, poty- and bymoviruses (Ryan and Flint, 1997). Picornaviruses alone are one of the largest and most important families of human and agricultural pathogens (Oliveira et al., 1999). Apart from being able to cause very severe acute diseases in humans, picornaviruses have also been indicated in some long term illnesses. For example, rhinoviruses are linked with induction and exacerbation of asthma, whereas enteroviruses, especially members of the coxsackievirus B group, have been linked with the development of type 1 diabetes (Hansbro et al., 2008; Hober and Sane, 2010; Jaidane et al., 2010; Johnston, 2005; Tauriainen et al., 2010; Walton and Johnston, 2008). Picornaviruses also infect live stock and for example, the foot-and-mouth disease virus (FMDV) is one of the most important pathogens of cloven-hoofed animals, it is highly contagious and it can cause severe economic losses (Grubman et al., 2008; Klein, 2009; Mardones et al., 2010). Furthermore, the picornavirus superfamily contains many agriculturally and economically significant plant viruses, for example tobacco ringspot virus (TRSV) and potato virus Y (Singh et al., 2008; Wang et al., 2002).

# 1. Capsid structure, assembly and cell entry of spherical members of the picornavirus superfamily

## 1.1. Why so symmetric?

Virus capsids are essentially protective shells that contain and protect the genome, until a suitable host is found, entered and the genome released (Smith and Helenius, 2004). The viral genome holds the information for producing all the necessary proteins, including the structural proteins, to make new virus capsids. As such, increasing the size of the capsid by increasing the size of the capsid proteins, inevitably leads to a larger genome. Thus a problem arises: how can a virus produce a capsid spacious enough to package the genome while maintaining a conservative use of nucleic acid. Viruses have resolved this dilemma by constructing their capsids from several copies of one or more small proteins (Caspar and Klug, 1962; Johnson, 1996).

Virus capsids are generally found to be either rod-shaped, spherical or pleomorphic (Casjens, 1997). The rod-shaped capsids, such as that of tobacco mosaic virus (TMV), display symmetry around the longitudinal axis and is referred to as having helical symmetry (Namba and Stubbs, 1986). Of all the possible symmetries capable of producing a closed spherical capsid, only icosahedral symmetry has been observed (Casjens, 1997). The diameter of icosahedrally-symmetric viruses has been observed to range from approximately 25 nm (e.g. parvovirus) to 500 nm (mimivirus) (Xiao et al., 2005b; Xie and Chapman, 1996).

## 1.2. Icosahedrally-symmetric capsids

Icosahedral symmetry is also referred to as ‘point group 532’ symmetry, as it contains five-fold, three-fold and two-fold axes of symmetry (Crowther, 1971b). Icosahedral symmetry is found in such geometrical constructions as icosahedrons and dodecahedrons (Baker et al., 1999). The icosahedron is a geometric construction that has 12 five-fold symmetric vertices, 20 three-fold symmetric facets and 30 edges with two-fold symmetry. The dodecahedron on the other hand has 12 five-fold symmetric facets, 20 three-fold symmetric vertices and 30 edges (Figure 1). The icosahedron is 60-fold symmetric, which means that the complete icosahedron can

be generated by the application of icosahedral symmetry elements if the asymmetric unit is known (Baker et al., 1999; Crowther et al., 1970). The asymmetric unit is a triangle that lies between two adjacent five-fold axes of symmetry and one adjacent three-fold axis of symmetry (Figure 1).

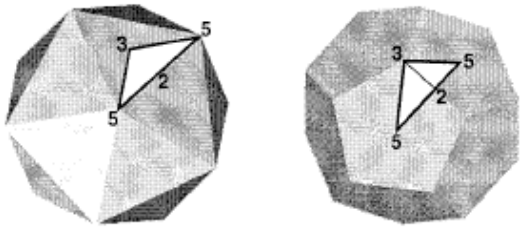


**Figure 1. Geometric representations of an icosahedron (left) and a dodecahedron (right). One two-fold (2), one three-fold (3) and two five-fold (5) symmetry axes are indicated along with the asymmetric unit that they define in both. Reprinted from (Baker et al., 1999) with permission from American Society for Microbiology.**

The icosahedrally-symmetric capsids are often described simply by supplying the triangulation number (T-number) (Caspar and Klug, 1962). The T-number is a geometric concept which arises when an icosahedron is folded from a two-dimensional lattice composed of hexagons. To fold an icosahedron out of a hexagonal lattice, 12 of the hexagons must be replaced with pentagons in correct positions (Baker et al., 1999; Crowther, 1971b). The T-number describes how the pentagons are placed in the hexagonal lattice. In the hexagonal lattice two axes (h and k) are defined (Figure 2). The separation of the pentagons on axes h and k gives rise to the related T-number according to the formula (1) (Baker et al., 1999; Caspar and Klug, 1962).

$$T = h^2 + hk + k^2 \qquad \textbf{(1)}$$

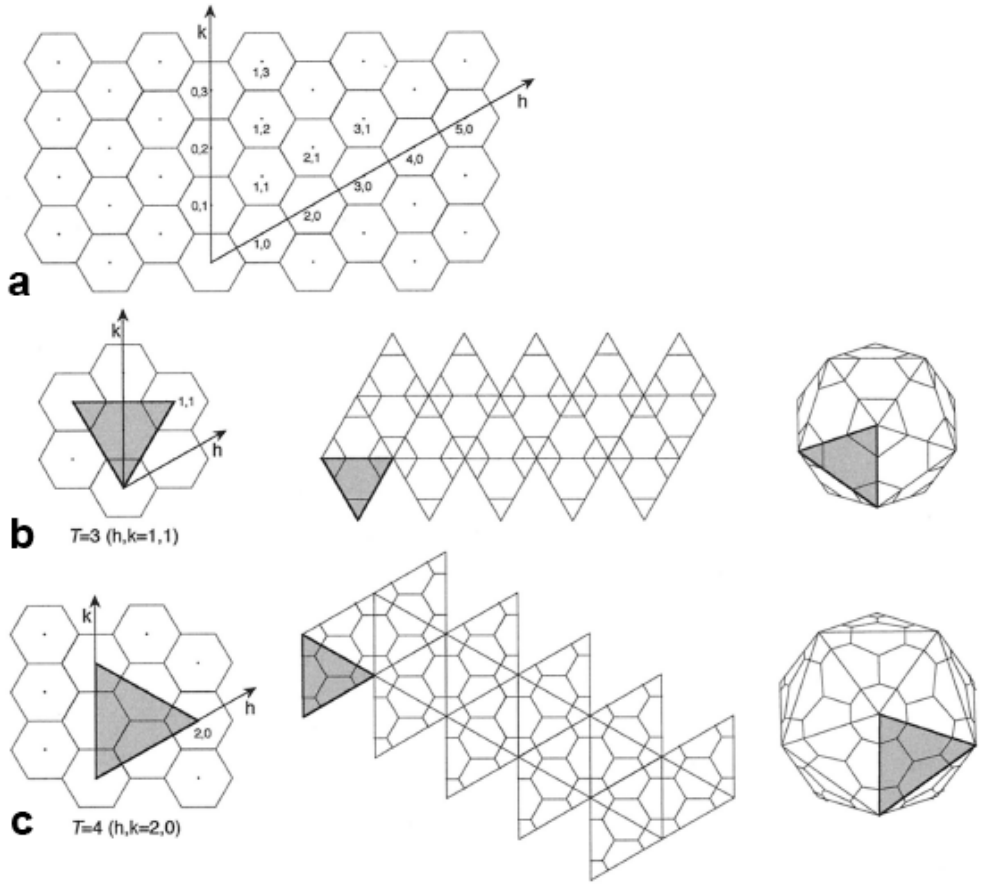


**Figure 2. Geometric principles of constructing icosahedral lattices of defined triangulation number. (a) A hexagonal lattice indicating the ordering of h- and k-axes. (b) Example of building a T=3 icosahedron from the hexagonal lattice, the (h,k)-coordinates for the correct position of the pentagon are indicated (1,1). (c) Example of building a T=4 icosahedron from the hexagonal lattice, the (h,k)-coordinates for the correct position of the pentagon are indicated (2,0). Modified from (Baker et al., 1999), with permission from American Society for Microbiology.**

Greater separation of the pentagons along the h and k axes leads to larger capsids for the same subunit. Thus, replacing all hexagons with pentagons leads to separation of one step (either in h or k) and correspondingly to T=1 characterization of the structure. The definition of the T-number predicts that only certain types of icosahedrally symmetric capsids are possible and for example no T=2 structures can exist (Baker et al., 1999; Caspar and Klug, 1962; Crowther, 1971b).

In icosahedral viruses the hexagons and pentagons are composed of the capsid proteins that assemble into the viral capsid (Crowther, 1971b). Thus, the T-number often allows one to predict the number of capsid proteins. The

simplest icosahedral capsid (T=1) has 60 copies of each of the capsid proteins, whereas the next allowed icosahedral capsid (T=3; h=1, k=1) has 180 copies (Caspar and Klug, 1962; Chandrasekar and Johnson, 1998; Crowther, 1971b). It is important to note that, although the proteins are identical in amino acid sequence, the interactions between the proteins are not necessarily the same for each copy (Caspar and Klug, 1962). In the simplest icosahedral capsid each asymmetric unit is composed of a single protein and all the interactions are identical. However, the assembly of a more complicated icosahedral capsid requires some of the proteins to adopt a slightly different environment usually through conformational flexibility and this leads to quasi-equivalence (Caspar and Klug, 1962).

However, some of the experimentally obtained virus structures contradict the theory developed by Caspar and Klug (Caspar and Klug, 1962). These contradictory cases include at least: polyoma virus, Simian Virus 40 (SV40) and L-A virus (Caston et al., 1997; Liddington et al., 1991; Rayment et al., 1982). In the case of polyoma virus and SV40 the theory by Caspar and Klug, while predicting the position of capsomers correctly, fails to predict the number of protein subunits correctly. Additionally, these experimental data illustrate that virus structures can have pentameric structures in positions where the theory predicts only trimeric or hexameric features (Caspar and Klug, 1962; Twarock, 2004). Furthermore, the experimentally obtained data reveals that the L-A virus exhibits the 'forbidden' T=2 organization. A newer theory, inspired by Penrose tilings, that allows a more generalized solution is able to correctly predict these structures (Twarock, 2004). The newer theory deviates from the older theory by allowing icosahedrally symmetric structures to be composed from elements other than triangles, for example rhombs (Twarock, 2006).

## 1.3. Genomic organization in picornavirus superfamily

The single-stranded (ss) RNA genomes of members of the picornavirus superfamily are around 8 kb in size and as such can only code for a minimal amount of proteins (Bedard and Semler, 2004; Ryan and Flint, 1997). The proteins encoded by the genome can be divided into structural and non-structural proteins. The structural proteins assemble to make up the viral capsid and the non-structural proteins contain at least proteases, VPg terminal proteins, helicases and

RNA dependent RNA polymerases (Bedard and Semler, 2004; Lin et al., 2009). The RNA is transcribed into a single polypeptide, which is then appropriately cleaved by the proteases to make the final protein products (Figure 3). The viral proteases are responsible for the cleavage of the polyprotein. The polymerases replicate the genome and the helicases separate positive RNA strands from the negative RNA strands. The VPg terminal protein binds to the 5' end of the plus strand RNA and participates in the replication of the genome (Bedard and Semler, 2004; Lin et al., 2009).

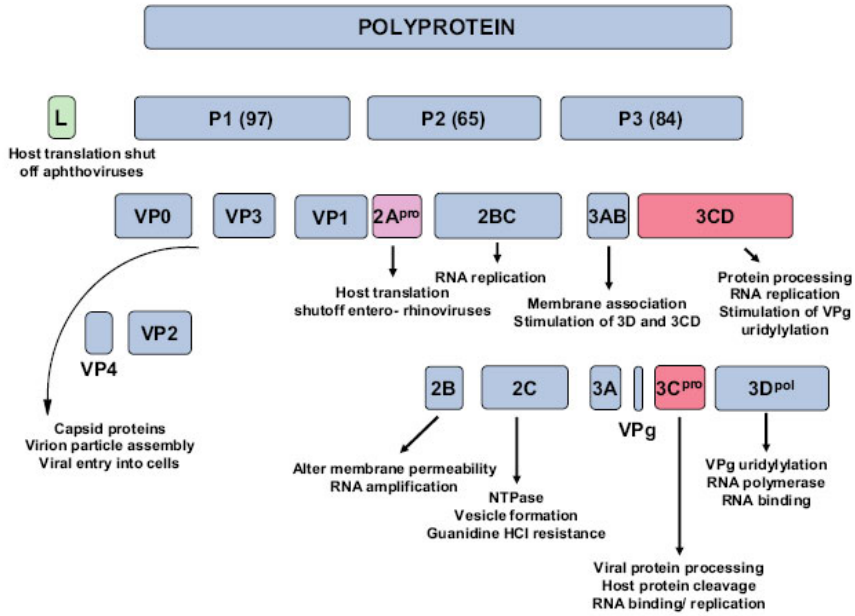


**Figure 3. Picornavirus polyprotein processing cascade. The processing schematic shows the precursor and mature polyproteins that result from cleavage by the three viral proteases. The functions of the precursor and mature polyproteins are indicated. Reprinted from (Bedard and Semler, 2004) with permission from Elsevier.**

## 1.4. Morphology and symmetry of picornavirus superfamily members

The members of the picornavirus superfamily exhibit considerable structural variation, as the superfamily contains both icosahedral and rod-shaped viruses (Ryan and Flint, 1997). However, the icosahedral members of the superfamily have structural characteristics similar to picornaviruses. Picornaviruses have icosahedral capsids made up of 60 copies of each structural protein and

no lipid membranes (Muckelbauer et al., 1995). Additionally, the icosahedral members of this superfamily have capsid diameters ranging between 300-330 Å (Fry et al., 1999; Hendry et al., 1999). Furthermore, all of the icosahedral viruses from the picornavirus superfamily, that have known structures, exhibit the simplest icosahedral symmetry, T=1 symmetry (Chandrasekar and Johnson, 1998; Hogle et al., 1985; Rossmann et al., 1985). However, many of the picornavirus animal pathogens have three different structural proteins in one asymmetric unit and are thus characterized with a pseudo-T-number (pT-number) instead, to describe the structure in more detail. The pT=3 structure describes the capsid as being made up of 60 copies of each of the three different capsid proteins (VP1, VP2 and VP3). Capsid protein VP4 is often considered non-structural, although it is present in the capsid. Most known plant viruses of the picornavirus superfamily on the other hand have only one structural protein, which folds in three separate domains, which is also sometimes referred to as a pT=3 structure (Chandrasekar and Johnson, 1998).

## 1.5. Common fold of the coat proteins

Proteins fold to form two types of secondary structures, α-helices and β-sheets. A β-sheet is formed when a protein strand loops around and the amino acids of the parallel or anti-parallel strands form hydrogen bonds. The β-sheets can then further curl to form β-barrels (Figure 4). The known structures of picornaviruses almost invariably reveal the capsid proteins to form 8-stranded β-barrels (Hogle et al., 1985; Krishnaswamy and Rossmann, 1990; Muckelbauer et al., 1995). As an exception the VP1 of FMDV forms a 7-stranded β-barrel (Acharya et al., 1989; Fry et al., 1993). In the case of viruses with more than one structural protein, each of the major structural proteins (VP1, VP2 and VP3) forms a β-barrel, thus effectively having three β-barrels per asymmetric unit (Hendry et al., 1999). The VP4, which is a smaller protein, is unable to form a β-barrel and often contains little secondary structure. In the case of the viruses with only one structural protein, the sole protein folds into three separate β-barrel domains (Chandrasekar and Johnson, 1998).

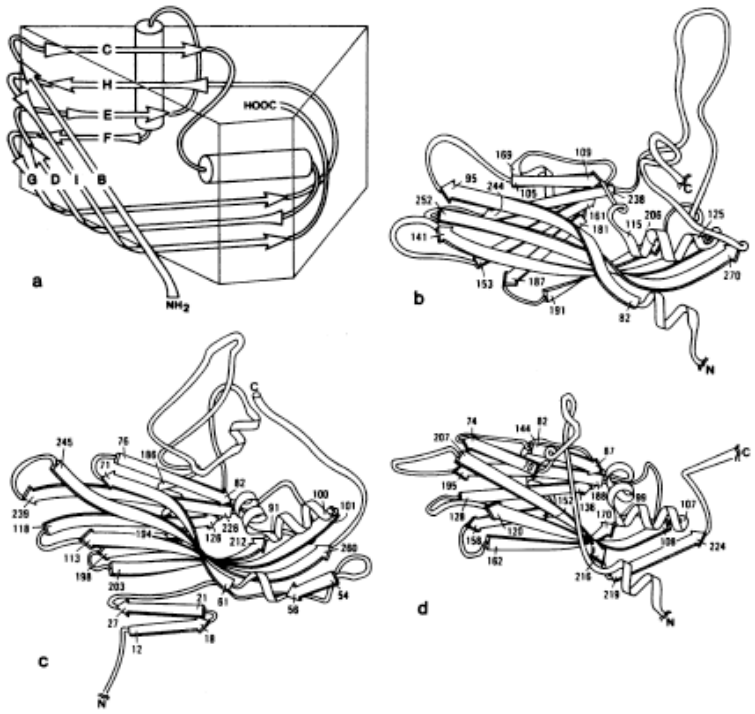


**Figure 4. Schematic representation of the poliovirus capsid proteins. (a) Simplified diagram showing the topology of the structurally conserved β-barrel structure. Ribbon diagrams illustrate the β-barrel fold of (b) VP1, (c) VP2 and (d) VP3. The $NH_2$- and COOH-terminal extensions of VP1 and the $NH_2$-terminal extension of VP3 have been truncated for clarity. Reprinted from (Hogle et al., 1985) with permission from AAAS.**

## 1.6. Assembly

The capsids of picornavirus superfamily members assemble without the help of additional molecules. Some picornaviruses can form assembly intermediates, for example poliovirus produces pentamers which cluster together to form the complete capsid (Watanabe et al., 1965). For poliovirus capsid at least two assembly routes have been suggested: co-assembly of the capsid and the genome, or alternatively the genome is packaged in to an empty precursory capsid (Ansardi et al., 1994; Basavappa et al., 1994). As no translocation active proteins have been detected in poliovirus, the suggested mechanism associates RNA packaging with autocatalytic maturation cleavage of VP0 (Basavappa et al., 1994; Levy et al., 2010). Poliovirus might also be able to use both pathways depending on the prevailing conditions. Presumably some form of

interactions between the capsid proteins and the genome must exist, as the capsid can selectively package the correct RNA segment to become infectious. It has been shown that the assembly of cowpea chlorotic mottle virus (CCMV) is RNA-dependent. No empty capsids are formed in native infection as the viral RNA initiates the capsid assembly (Fox et al., 1998). As with poliovirus, the assembly of CCMV has been shown to proceed through pentameric assembly intermediates (pentamers of dimers) (Zlotnick et al., 2000).

Perhaps the most comprehensive model of co-assembly is available for bacteriophage MS2 (Basnak et al., 2010; Dykeman et al., 2010; Morton et al., 2010; Rolfsson et al., 2010). The bacteriophage MS2 has an organized ssRNA genome enclosed in a T=3 capsid (Convery et al., 1998; Toropova et al., 2008; Valegård et al., 1994; Valegård et al., 1997). The MS2 capsid is made up of 90 non-covalently bound dimers which exist in two forms, the symmetric and the non-symmetric (Golmohammadi et al., 1993). The binding of a specific RNA stem loop triggers the formation of the non-symmetric dimer from the symmetric dimer (Stockley et al., 2007). The strongest interactions between dimers occur between a symmetric dimer and a non-symmetric dimer. Additionally, an intermediate formed by two RNA stem loop bound dimers is likely to be a dead end assembly pathway (Morton et al., 2010). Thus, protein-RNA interactions are directing the assembly by stabilizing intermediates on the correct pathway and blocking the ones on the wrong pathway. The dimers have been observed to assemble further in to hexameric and decameric intermediates. The current model of MS2 assembly sheds light on the importance of interactions between RNA and capsid proteins in directing the assembly towards the correct capsid structure.

## 1.7. Host-cell infection

As all viruses are obligate parasites, each virus must manage the critical step of entry in to a host cell (Pelkmans and Helenius, 2003; Roth et al., 2004; Smith and Helenius, 2004). The entry mechanism depends heavily on the host, species, the host cell type as well as the species of the virus. Similarly, the subsequent steps leading to successful viral replication and release are also host and virus specific (Klein, 2009; Lin et al., 2009). The specificity required for successful cell entry and the subsequent replication effectively prohibits viruses from freely migrating from one species to

another. Still some viruses have an enormous range of hosts, for example cucumber mosaic virus has a host range of about 1200 species, whereas the only known host of poliovirus is man (Minor, 1996; Roossinck, 2010). More detailed description of cell entry will be presented in later sections that focus on poliovirus 1 and human rhinovirus 14.

Plant virus entry is relatively simple; in natural settings the virus is often inserted in the plant by a vector (Shaw, 1999; Wang et al., 2002). Alternatively, entry may occur through damaged surface of the plant, which has been exploited in laboratory conditions to infect plants (Shaw, 1999). Once the virus has entered a suitable cell the infection commences and the cell starts producing viral proteins and viral genome. The infection then proceeds to adjacent cells and may eventually lead to a systemic infection of the whole plant via the phloem (Loebenstein, 2009; Roth et al., 2004). In the case of insect vectors, the disease is then transmitted further when a suitable vector feeds on an infected plant, ingests mature viral particles and later feeds on another susceptible plant. Hence affinity for an insect vector that feeds exclusively on suitable host plants is advantageous for the virus. Additionally, it has been suggested that the nematode-borne viruses are required to dissociate from virus-retention sites of the vector, prior to the successful infection of the next host plant (Wang and Gergerich, 1998; Wang et al., 2002). Selection for the proper vector is conveyed by the capsid of the virus and mutations in the structural proteins have been shown to severely affect plant virus vector transmission (Atreya et al., 1991; Harrison et al., 1974; Mayo et al., 1974).

In the picornaviruses infecting animals, the structure of the capsid plays a key role in cell entry. For successful cell entry, the viral capsid must identify and bind the correct cellular receptor(s) which then mediate entry by triggering the uptake mechanisms of the cell (Mercer et al., 2010; Smith and Helenius, 2004). Some picornaviruses require an additional receptor or receptors to trigger the uptake mechanism, whereas others, such as poliovirus, utilize the same receptor for initial recognition and signaling (Coyne and Bergelson, 2006; Hogle, 2002; Nemerow, 2000).

Viruses infecting mammalian cells utilize a multitude of pathways for cell entry (Smith and Helenius, 2004). Of non-enveloped viruses, such as picornaviruses, many require one of the endocytic pathways (Figure 5) (Marsh and Helenius, 2006). The clathrin-mediated pathway is the most commonly observed pathway utilized by viruses. Additionally, picornaviruses such as echovirus1 and coxsackievirus B3 are known to use the caveolar pathway (Coyne

and Bergelson, 2006; Pietiäinen et al., 2004). Once the cell is entered viruses require proper conditions to initiate the uncoating of the genome. For some viruses binding of the correct receptor is enough to initiate uncoating, whereas others require otherwise suitable conditions, such as low pH (Arita et al., 1998; Nurani et al., 2003). If the conditions are not met, the infection is not successful. The strict requirements for a correct receptor are one reason for host species specificity as the receptors vary from species to species. The receptor specificity also directs the virus into certain tissues of the infected animal as different tissues express receptors in different quantities.

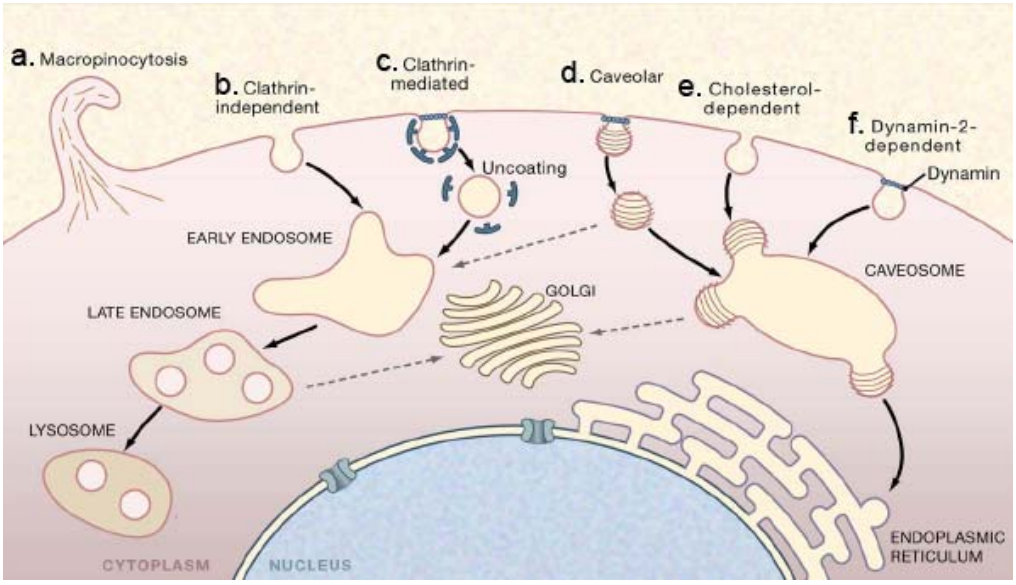


**Figure 5. Endocytotic pathways used by viruses infecting animal cells. (a) Macropinocytosis is involved in the entry of adenoviruses. (b) A clathrin-independent pathway from plasma membrane has been shown to exist for influenza virus and arenaviruses. (c) The clathrin-mediated pathway is the most commonly observed uptake pathway for viruses. (d) The caveolar pathway is one of the several closely related, cholesterol-dependent pathways that bring viruses to caveosomes, from which many of them continue to the ER, by a second vesicle transport step. (e) A cholesterol-dependent endocytotic pathway devoid of clathrin and caveolin-1. (f) A pathway similar to (d) except dependent on dynamin-2. Depending on the virus and cell type, penetration reactions occur in five locations: the plasma membrane, early and late endosomes, caveosomes and the ER. The additional endocytotic mechanism of phagocytosis also operates in many cells but has not as yet been linked to virus entry and is not included here. Modified from (Marsh and Helenius, 2006) with permission from Elsevier.**

# 2. Select members of the picornavirus superfamily

Several of the members of the picornavirus superfamily are significant for the human population. Among the best studied are the serotypes of poliovirus, which are members of the human enterovirus group C (HEV-C). Of the three serotypes, it is poliovirus 1 (PV1) that has been most extensively studied. Additionally, the successful vaccination campaign against the serotypes of poliovirus offers an interesting example of an eradication campaign and the difficulties likely to affect similar campaigns in the future (see Section 2.1). Another well studied virus in the picornavirus family is rhinovirus, which is a member of the human rhinovirus group B (HRV-B). Several of the serotypes have been well studied, but human rhinovirus 14 (HRV14) was the first picornavirus structure that was resolved at atomic resolution (Rossmann et al., 1985). Many of the proposed mechanisms of picornaviruses are derived from the wealth of information made available by the poliovirus and rhinovirus studies. On the other hand, enterovirus 71 (EV71) is a relatively little studied virus, but one that is the subject of many scientific inquiries at the moment. EV71 is a member of the human enterovirus group A (HEV-A) and the causative agent of an epidemic circulating in Asia since 1997, causing severe symptoms in many of the infected human beings (Ang et al., 2009; Tee et al., 2009; van der Sanden et al., 2009). As such EV71 is a strong candidate for vaccine development and a possible candidate for the next large scale vaccination campaign. Although, many structures of plant viruses are available, the only member of the nepovirus family to be structurally studied to atomic resolution is TRSV (Chandrasekar and Johnson, 1998).

## 2.1. Poliovirus 1

Poliovirus 1 is the most comprehensively studied picornavirus to date in the world. PV1 has been a subject of scientific enquiries since 1908 when it was identified as the cause of poliomyelitis (Racaniello, 2006). The poliovirus epidemic is considered to have started with the improvement of overall hygiene in the western countries. Before the improvement in hygiene poliovirus was first contracted in early infancy while still under the protection of maternal antibodies. Poliomyelitis causes irreversible damage to the

nervous system causing temporary or permanent neural damage of varying severity in 0.1–1 % of patients (Ehrenfeld et al., 2009). The battle against poliomyelitis started in 1955 with the formalin-inactivated poliovirus vaccine (IPV) developed by Jonas Salk (Salk et al., 1954a; Salk et al., 1954b). Three monovalent live-attenuated oral poliovirus vaccines (OPV) developed by Albert Sabin were licensed for use in 1961 (Sabin et al., 1954). In 1963 trivalent OPV providing coverage for different poliovirus serotypes was introduced and Salk IPV was quickly replaced in routine vaccinations. The war waged on polio has been successful in most countries worldwide, but there have been some setbacks and the war is still waged in some countries where polio eradication has not been successful.

The OPV vaccine widely used carries the burden of the attenuated virus reverting back to neurovirulence in approximately 1 per 750 000 cases. Vaccine derived poliovirus (VDPV) has been responsible for a few epidemics around the world. The VDPV epidemic in Hispaniola in 2000 was traced to Sabin OPV type 1 virus which had recombined with an unidentified Group C enterovirus and regained neurovirulence (Kew et al., 2002). If the proportion of vaccinated population is low, a recombined poliovirus can propagate efficiently and start an epidemic. Additionally, the ability of OPV strains to revert back to neurovirulence has led to opposition to the vaccine in some regions. Currently the greatest obstacles in OPV distribution are logistical problems, regional wars and resistance of the population against vaccinations. These issues make delivering the vaccine to everyone a difficult task. Overall the battle against polio could not have been this successful unless the vaccine was relatively easy to produce and the effects were long-lasting/permanent. The long-lasting effect of the vaccine is most likely due to the inability of polioviruses to mutate the antigenic parts of their protein shell, whereas some viruses undergo constant mutations to avoid detection by the immune system e.g. influenza viruses.

Poliovirus 1 utilizes CD155 as a receptor for cell entry (Mendelsohn et al., 1989). Binding to CD155 is the first step of PV1 cell entry and binding of CD155 to PV1 is known to initiate conversion of native 160S particles to altered 135S particles in physiological temperatures (Arita et al., 1998). The 135S particles expose transiently the hydrophobic C-termini of the VP1, the VP4 molecules become externalized and embedded in the cell membrane (Danthi et al., 2003; Fricks and Hogle, 1990). Following steps lead to internalization via an endocytotic pathway, although the exact pathway remains unclear (Basavappa et al., 1994; DeTulleo

and Kirchhausen, 1998). Subsequently, the RNA genome is released through a pore opened into the endosomal membrane and the 135S particles are converted to 80S particles devoid of RNA (Arita et al., 1998). It has been proposed that the pore-forming proteins are VP4 and the N-termini of VP1 (Tuthill et al., 2006). The only RNA density present in the native PV1 capsid X-ray structures is found associated with the amino-terminal residues of VP2 (Levy et al., 2010). However, biochemical studies have shown that a single point mutation in either one of the capsid proteins VP3 or VP4 can inhibit packaging of RNA, while allowing empty capsid assembly (Ansardi et al., 1994). Furthermore, the PV1 VP4 and the N-termini of VP1 are positioned on the inside of the capsid, near the strongest sign of capsid protein-RNA interaction site of cryoEM model EMD-5144.

Studies of poliovirus 1 have yielded a wealth of information, including an abundance of structural information. It is due to the combination of biochemical and structural data that we have a working model of poliovirus cell entry. The structure of the 160S form of PV1 was solved to 2.9 Å resolution in 1985 and subsequently to 2.2 Å resolution in 2001 by X-ray crystallography (Hogle et al., 1985; Miller et al., 2001). The structure of PV1 complexed with CD155 was solved to 15 Å resolution in 2003 and later to 8 Å resolution in 2008 using cryoEM (He et al., 2003; Zhang et al., 2008a). The 135S cell entry intermediate of PV1 has been solved to 10 Å resolution using cryoEM and the 73S empty capsid to 2.88 Å resolution using X-ray crystallography (Basavappa et al., 1994; Bubeck et al., 2005). Additionally, the early and late 80S forms have been solved to 10 Å resolutions using cryoEM (Levy et al., 2010). In addition to the structures listed above, structures of several mutant PV1 and antibody bound PV1 have been solved. The structural studies of intermediate forms of the PV1 capsid have provided detailed information on which amino acid residues are critical for the interaction PV1 capsid and CD155 receptor and what conformational changes occur in the PV1 capsid during the uncoating steps.

## 2.2. Enterovirus 71

Enterovirus 71 was first isolated and described in California in 1974 and it is one of the most prominent picornaviruses of humans today, causing major epidemics in Asia for over ten years now (Lee and Chang, 2010; Schmidt et al., 1974). Between 1975 and 2009 epidemics involving EV71 have been reported in Europe as well (Chumakov et al.,

1979; van der Sanden et al., 2009). The most common symptoms of EV71 infection are fever and hand, foot, and mouth disease where typically oral ulcers and rashes in the extremities develop. The extreme consequences of EV71 infection, which are flaccid paralysis or even death, appear to affect mostly children (Chan et al., 2000; Ho et al., 1999). The severe symptoms of EV71 infection in childhood have been associated with adverse effects in neural development (Chang et al., 2007). The disease caused by EV71 can resemble poliomyelitis in nearly every respect (Chumakov et al., 1979). Studies of EV71 are still ongoing, but it seems that the rate of severe symptoms is comparable to that of different poliovirus serotypes (Arita et al., 2007). During the past ten years EV71 has also been mutating rather quickly giving rise to the possibility that EV71 may become a successor of polio.

These considerations make EV71 a prime candidate for vaccine development and a vaccine against EV71 is currently under active development in Asia. Some promising vaccine candidates, consisting of inactivated virus, attenuated virus, virus-like particles or capsid subunits, have been discovered and a vaccine against EV71 may become available in the next five to ten years (Arita et al., 2007; Arita et al., 2005; Chung et al., 2008; Wu et al., 2002). Recent studies have shown that EV71 utilizes sialylated glycans, P-selectin glycoprotein ligand-1 and scavenger receptor B2 as cellular receptors (Nishimura et al., 2009; Yamayoshi et al., 2009; Yang et al., 2009). Identification of these receptors may prove helpful for vaccine development and also for understanding the tissue tropism of EV71. EV71 is a member of the HEV-A group and currently there is no structural data available on any of the members of that group.

## 2.3. Human rhinovirus 14

Rhinoviruses are divided into a minor and a major group depending on the cellular receptor they employ to enter the cell (Uncapher et al., 1991). HRV14 is a member of the major group rhinoviruses which bind to intracellular adhesion molecule 1 (ICAM-1). Additionally, HRV14 is one of the best studied picornaviruses along with PV1. HRV14 infections often lead to respiratory illnesses and it is one of the many causes of the common cold (Hayden, 2004). The sheer number of rhinovirus serotypes has made the development of a vaccine against rhinovirus-induced diseases very difficult. Additionally, the symptoms of rhinovirus infections are generally so mild that the

development a vaccine preventing infection is not of such high priority as the polio vaccine was in the 1960s. However, studies performed on HRV14 provide further insight into the cell entry and uncoating mechanisms of picornaviruses (Goncalves et al., 2007; Grunert et al., 1997; Katpally and Smith, 2007; Khan et al., 2010; Nurani et al., 2003; Rossmann, 1994).

The cell entry of HRV14 has been determined to enter rhabdomyosarcoma cells in a manner that is independent of clathrin, caveolin and flotillin, and resembles macropinocytosis (Khan et al., 2010). However, HRV14 seems to utilize an endocytotic pathway when infecting HeLa cells (Grunert et al., 1997). These studies indicate that cell entry pathway of a given virus may vary depending on the cell type. Furthermore, HRV14 as model system, along with PV1, allow better understanding of common themes in picornavirus life cycles, as well as the differences in them.

The uncoating mechanism of the endocytotic pathway of major group rhinoviruses is similar to that of PV1. Binding of the cellular receptor initiates entry and uncoating (Bayer et al., 1999). However, low pH in addition to the receptor binding facilitates uncoating (Nurani et al., 2003). The VP4 protein of HRV14 is externalized or released and the C-termini of VP1 is exposed and together they interact with the endosomal membrane to allow release of the RNA genome in to the cytosol (Hoover-Litty and Greve, 1993). The release of VP4, prior to binding with ICAM-1, renders HRV14 particles uninfectious. The anti-viral compounds developed against rhinoviruses, known as the WIN compounds, bind to rhinovirus particles, so that either the binding of ICAM-1 is blocked or the VP4 protein cannot be released (Goncalves et al., 2007; Hadfield et al., 1995; Smith et al., 1986).

## 2.4. Tobacco ringspot virus

The genome of TRSV is bipartite positive-sense single-stranded RNA. One segment (RNA1) codes the non-structural proteins and the second (RNA2) codes for the capsid protein and a movement protein (Forster and Morris-Krsinich, 1985; Jobling and Wood, 1985). The genome segments are packaged in separate particles and both segments are required for infection (Diener and Schneider, 1966) (Murant et al., 1981). TRSV is not limited to tobacco as a host and is capable of causing such diseases as soybean budblight, ringspot diseases of tobacco and cucumber, and chlorotic or necrotic

spotting in many annual and perennial crops (Chandrasekar et al., 1997).

The TRSV capsid protein has been expressed in insect cells and subsequently the structure of the TRSV virus-like particle, a particle composed of native virus capsid proteins but assembled without RNA encapsidation, has been solved by cryoTEM (Singh et al., 1995). The native virus structure of TRSV has been solved by X-ray diffraction (Chandrasekar and Johnson, 1998). The TRSV capsid is 280 Å in diameter and is made up of 60 copies of a single structural protein. The structural protein has a molecular weight of 56 kDa and it folds to form three β-barrel domains. The density corresponding to RNA is not visible in the X-ray structure due to asymmetric distribution in the capsid. Additionally, even though RNA density is generally visible in cryoEM structures of icosahedral viruses, the density does not represent the native distribution of RNA, but only the average of the icosahedrally symmetric RNA.

# 3. Viruses in this study

## 3.1. Blackcurrant reversion virus

Blackcurrant reversion virus (BRV) is an important pathogen of commercial blackcurrant crops. BRV has been shown to be the causative agent of blackcurrant reversion disease (BRD) (Lemmetty et al., 1997; Lemmetty and Lehto, 1999). BRD occurs worldwide with the exception of the Americas (Jones, 2000). The disease occurs in two different forms of which the more severe one affects Scandinavia, Eastern Europe and countries of the former Soviet Union (Jones and McGavin, 2002).

The virus itself spreads from one plant to next via an insect vector, the eriophyid mite *Cecidophyopsis ribis* (Thresh, 1964). BRV is the only member of the nepovirus group transmitted by mites. BRV is transmitted between the blackcurrant plant and the mites as the mites feed on the plant. The first symptoms of BRD typically appear 1-2 years after the initial BRV infection (Jones, 2000). Initially the symptoms involve deformation of leafs and flowers. Eventually the infection progresses to complete sterility stopping the plant from bearing any fruit (Jones, 2000).

BRV has a bipartite positive sense RNA genome that encodes a single capsid protein (Latvala et al., 1998). The capsid protein of BRV has been observed in two forms with

molecular weights of 54 and 55 kDa. The N-termini of the differently sized proteins are identical (Lemmetty et al., 1997). Containment of BRV infection in a blackcurrant farm is a very difficult task, as the symptoms take a long time to become apparent. Additionally, the wind-dispersed mites are capable of spreading the disease quickly from plant to plant. Currently the only effective method of purging BRV infection from a blackcurrant farm is to replace all the plants at once. Identification of the mite-specific segment of the BRV capsid protein might provide means to limit the transmission of BRV from infected plants to healthy plants in the future. Thus, only the diseased plants would need to be removed, allowing a less wasteful method of purging BRV from a farm.

## 3.2. Human parechovirus 1

Human parechovirus 1 (HPEV1) was originally known as echovirus 22, but later genome analysis revealed significant differences in comparison to other picornaviruses and thus it was reclassified as HPEV1 (Hyypiä et al., 1992). HPEV1 is a very common human pathogen worldwide. The majority of HPEV1 infections occur in early childhood and are mild gastrointestinal or respiratory illnesses (Joki-Korpela and Hyypiä, 2001). However, HPEV1 can cause infections of the central nervous system, myocarditis and generalized infections in neonates which are serious medical conditions (Stanway et al., 2000).

HPEV1 differs from most other known picornaviruses as it lacks the cleavage of VP0 protein into VP2 and VP4 (Stanway et al., 1994). This maturation cleavage stabilizes the virion and is considered a necessary step for polioviruses (Basavappa et al., 1994). To date, the only other picornavirus that lacks this cleavage is the Aichivirus (Yamashita et al., 1998). Similarly to coxsackievirus A9 (CAV9) and echovirus 9 (EV9, Barty strain) HPEV1 has an arginine-glycine-aspartic acid (RGD) motif at the C-terminus of VP1 (Chang et al., 1989; Hyypiä et al., 1992; Zimmermann et al., 1996).

Mutations in the RGD-motif of CAV9 are found to affect virus titres and the range of tissues where CAV9 is recovered from (Harvala et al., 2003). Whereas, neither CAV9 nor EV9 infection is completely dependent of an intact RGD-motif, deletions in the RGD-motif have been shown to be lethal for HPEV1 (Boonyakiat et al., 2001; Hughes et al., 1995; Zimmermann et al., 1995). For CAV9, studies have identified integrin $\alpha_V\beta_3$ as a cellular receptor and shown that HPEV1 competes with CAV9 for this receptor,

indicating that HPEV1 employs the same receptor (Roivainen et al., 1994). Integrin $\alpha_V\beta_6$ has been identified as another RGD-dependent cellular receptor of CAV9 (Williams et al., 2004). Furthermore, integrin $\alpha_V\beta_1$ and matrix metalloproteinase 9 have been identified as cellular receptors of HPEV1 (Pulli et al., 1997). The interaction of RGD-motif with integrin $\alpha_V\beta_3$ has been structurally characterized and the interacting residues identified (Xiong et al., 2002). Studies on HPEV1 cell entry have indicated clathrin-dependent endocytic pathway as the entry route of HPEV1 (Joki-Korpela et al., 2001).

## 3.3. Coxsackievirus A7

Coxsackievirus A7 (CAV7) is member of the human enterovirus A group. CAV7 has been responsible for small scale epidemics in the USSR in 1952 and 1956, as well as in Scotland in 1959 and 1963 (Grist and Bell, 1984). Symptoms of a CAV9 infection include at least aseptic meningitis and paralysis, which is why it was originally named poliovirus type 4 in the USSR (Grist, 1962; Habel and Loomis, 1957). CAV7 was once considered the most important paralysis causing picornavirus, after poliovirus (Grist, 1969). However, CAV7 has been rarely encountered after the epidemics in the 1960's (Blomqvist et al., 2008). Several isolates of CAV7 were obtained during the epidemics in 1950's and 1960's and later one more in 1971 (Richter et al., 1971). The different strains of CAV7 exhibit differences in pathogenesis in mice and monkeys (Habel and Loomis, 1957; Richter et al., 1971). Interestingly, accumulation of haemagglutinin in CAV7 infected mouse tissues has been reported, but the purpose of the accumulation remains unclear (Williamson and Grist, 1965). The CAV7-Parker strain has been sequenced recently (Oberste et al., 2004). However, the cellular receptors of CAV7 have not been identified yet and no structural data for any member of the HEV-A group is available.

# B. AIMS OF THE PRESENT STUDY

For this study we chose members of the picornavirus superfamily as they commonly affect human lives either directly or through food production. The members of the picornavirus superfamily are numerous and there are still branches which have not been structurally characterized. Detailed knowledge of the virus structure is necessary to rationally design anti-viral compounds to combat the infections caused by viruses. The viruses studied in this study include BRV, which is the most significant pathogen of blackcurrant crops, CAV7 which was once considered the most significant paralysis-causing member of the enterovirus genus after poliovirus and HPEV1 which infects humans very efficiently and may become a major threat to the health of humans through recombination. The study was conducted to gain insight on the structural determinants vital for virus transmission and initiation of infection, which are events that offer potential targets for anti-viral compounds.

The aim was to use cryoEM and icosahedral image reconstruction to determine the structures of three viruses and the structures of additional states such as empty capsids or capsids complexed with their host receptors. We also wanted to combine homology models or X-ray structures to our results for more detailed analysis of the structures. The specific aims were:

**1.** To solve the structure of BRV and look for structural similarities to TRSV which, based on amino acid sequence, is the closest relative of BRV where an X-ray structure is available. The goal was that the structure could be used to model putative vector transmission sequences on the capsid proteins. Furthermore, we wanted to confirm, using antibodies that the smaller form of the capsid protein of BRV is due to C-terminal truncation of the capsid protein (Study I).

**2.** To solve the structure of HPEV1 as the first example of the parechovirus group, to compare the structure to other known picornavirus structures and correlate any similarities or differences with amino acid sequence comparisons. We also sought to identify receptors for the virus with infectivity studies, to solve the structures of HPEV1 complexed with those receptors and to locate the receptor-binding site on the viral capsid. The involvement of the RGD-motif in the receptor binding was to be confirmed with peptide blocking assays (Study II).

**3.** To sequence a number of CAV7 isolates, to solve the first

structure of a representative isolate as the first example in the enterovirus A group, and to map differences in the capsid proteins to try to understand the differences in pathogenicity at the structural level (Study III).

# C. MATERIALS AND METHODS

## 1. Cryo-electron microscopy and image processing

### 1.1. The electron microscope

Unlike light microscopes, which function in the visible light spectrum, the electron microscope uses electrons for probing the sample. The electrons are extracted from an electron source, which can be either a metal filament or a field emission gun (FEG) tip. In effect the metal filament is a metal wire, similar to those found in light bulbs. To extract electrons the filament is subjected to a significant amount of heat. The material commonly used for the filament is either tungsten or lanthanum-hexaboride ($LaB_6$). The FEG tip, on the other hand, is a carefully shaped piece of solid tungsten. Additionally, a specific type of FEG tip, named Schottky type, is coated with zirconium oxide to enhance thermionic emission at high temperatures. Regardless of the type, the electron source is heated to lower the energy barrier of electron extraction while maintained in an electric extraction potential. The extracted electrons are then accelerated with another electric potential, acceleration potential, to relativistic velocities. Electron sources must also be maintained in a vacuum or else they will degrade very rapidly.

Although, the process of electron extraction is similar in the case of either electron source, using a FEG tip has a few significant advantages. The temperature required for electron extraction is significantly lower, which slows the degradation of the tip. More importantly the electron beam produced with a FEG source is highly coherent and bright, which is important for imaging of biological samples which give weak and diffuse scattering (Orlova and Saibil, 2004). The use of electrons for sample probing is a cause for few other considerations. Firstly, electrons interact strongly with matter; therefore it is necessary to maintain a vacuum throughout the electron beam column. Secondly, the electron beam is controlled with magnetic lenses which, in comparison to glass lenses, are fairly difficult to shape accurately.

Thus, when compared to the lenses used in optical microscopes, the magnetic lenses are inferior and cause more distortion in the image.

## 1.2. Preparation and imaging of vitrified samples

Biological samples often contain water, which is problematic as the electron microscope column must be maintained in a vacuum and liquid water would dissipate quickly in those conditions. Thus it is necessary to fix the samples before they can be inserted in a transmission electron microscope (TEM). This can be achieved by cooling the sample so that the water solidifies. Three kinds of solid water exist at low pressure: hexagonal ice, cubic ice and vitreous water (Dubochet et al., 1988). Crystal formation in the sample would impose forces on the proteins distorting and disrupting them. Thus, the vitreous state of water is necessary to protect the sample from the vacuum and to preserve the native state of the proteins as much as possible.

Vitrified cryo samples are prepared using a so-called “plunging method” (Adrian et al., 1984; Baker et al., 1999). In this method a holey carbon coated copper grid is fixed to a pair of forceps, which in turn are attached to a guillotine-like device. A small amount of the sample (2-5 µl) is applied to the suspended grid and excess sample is then blotted away with a piece of filter paper, with the objective of leaving a thin film (~200 nm or less) of the sample in the holes. The thin layer of sample is essential, as to achieve the vitreous state of water; a temperature of -140 °C must be reached rapidly throughout the sample. The guillotine is released and the grid is plunged into a cryogen, usually liquid ethane or propane, which cools the sample rapidly (Dubochet et al., 1988). Liquid ethane or propane is used initially in the plunging step, as nitrogen has too low a heat capacity to allow rapid cooling. The low specific heat capacity of nitrogen causes boiling of nitrogen in the immediate vicinity of the sample and causes slow cooling; this is also known as the Leidenfrost effect (Baker et al., 1999). Treatment of the grids with a glow-discharge unit or a plasma cleaner prior to sample application leaves the grid surface charged, effectively rendering the grid surface hydrophilic. This is helpful because water is a polar molecule and the hydrophilic surface allows water to spread more evenly on the grid surface, whereas on hydrophobic surfaces water tends to form small droplets. Using the treated grids for sample preparation increases the chances of successful grid preparation significantly. Once the grid is prepared it is stored in a

holder, which in turn is placed in liquid nitrogen for storage.

For imaging purposes the grid is removed from storage and attached to a specific cryo-holder. The cryo-holder has a liquid nitrogen dewar at one end to keep the sample at the other end cooled below -140 °C for the duration of imaging. If the sample is heated above -140 °C, the vitrified water undergoes a phase transition to a crystalline phase (cubic or hexagonal ice is formed) and the formation of crystalline structure compromises the native state of the sample (Figure 6) (Adrian et al., 1984; Dubochet et al., 1988). The phase transition of water is an irreversible event and cooling the sample below the phase transition threshold temperature does not recover the amorphous state. The cool temperatures also provide cryo protection for the sample, as biological materials are very sensitive to the electron beam (Hayward and Glaeser, 1979). At liquid helium temperatures a dose of 20 to 230 $e^-/Å^2$ (electrons per angstrom squared), depending on the molecule, has been reported to reduce the first order reflections of protein crystals to 1/e (~37 %) of their initial values (Knapek and Dubochet, 1980). Once the electron dose starts to accumulate the biological materials are degraded and the fine structural details are the first ones to suffer. The maximum total dose which is generally considered safe is 20 $e^-/Å^2$ (Baker et al., 1999). The electron dose is regulated by using a low-dose setup which minimizes the exposure of areas which are imaged. In low-dose mode the grid is searched at a low magnification, where the electron dose is low and does not damage the sample very quickly. The actual area of interest is exposed with the intense beam only when data is collected. Other operations, such as focusing and beam adjustments, are performed in an area adjacent to the area of interest.

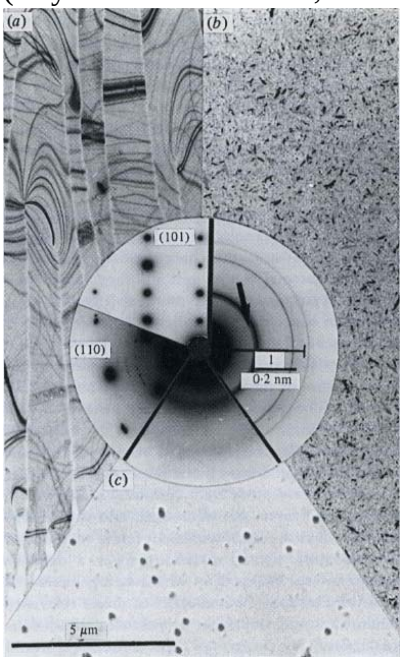


**Figure 6. Typical images and electron diffraction patterns of three forms of solid water observed in the electron microscope. (a) Hexagonal ice obtained by rapid freezing of a water layer on a carbon film. The diffraction patterns, obtained from other specimens, show the (110) and (101) plane. (b) Cubic ice obtained by warming a layer of vitreous water obtained by condensation. The shoulder on the (111) reflection, possibly indicates a small amount of hexagonal ice (arrow). (c) Vitreous water obtained in the microscope, by condensation of vapor on a cold carbon film supporting polystyrene spheres. Reprinted from Dubochet et al. (1982) with permission from Royal Microscopical Society.**

## 1.3. Image formation and contrast transfer

The image in transmission electron microscope is formed by electrons passing through the sample. The electrons are guided and focused by magnetic lenses inside a column that is maintained in a high vacuum state. The electrons scatter from the sample via processes known as elastic and inelastic scattering. The elastically scattered electrons do not lose momentum due to the scattering, whereas the inelastically scattered electrons lose momentum. The inelastic electrons are an undesired, yet unavoidable outcome, as they are a source of noise in the final image (Schröder et al., 1990). The amount of inelastic electrons passing to the image plane can be reduced through the use of apertures, which are metal plates with a small hole in them. The electrons that have scattered in a wide angle do not pass through the hole. This is a routine method used in TEM imaging. However, this method is unable to remove the inelastic electrons that scatter in a narrow angle. However, the inelastically scattered electrons carry less momentum compared to the elastically scattered electrons and thus they can be further prevented from reaching the image plane by the use of an energy filter (Angert et al., 2000; Schröder, 1992).

After being scattered by the sample, electrons pass through apertures and are focused on the image plane by the objective lens. The image formed on the plane is composed of two components, the amplitude contrast and the phase contrast. In cryo transmission electron microscopy (cryoTEM), it is the phase contrast that is the dominant component in the final image. The fraction of amplitude contrast is around seven percent (Toyoshima and Unwin, 1988). The behavior of phase contrast is described by the contrast transfer function (CTF) which is described by the formula (Baker et al., 2000):

$$CTF(\nu) = -\{1 - F_{amp}^{2})^{1/2} \cdot \sin(\chi(\nu)) + F_{amp} \cdot \cos(\chi(\nu))\} \cdot e^{-(\delta\nu)^2} \quad \textbf{(2)}$$

Where $sin(\chi(\nu))$ is the phase contrast element, $cos(\chi(\nu))$ is the amplitude contrast element, $F_{amp}$ is the fractional amplitude contrast and $e^{-(\delta\nu)^2}$ describes the attenuation of the signal as a function of spatial frequency ($\nu$) and beam coherence ($\delta$). Function $\chi(\nu)$ is a phase shift function which describes the aberrations introduced to the object transform due to the imperfections in the electron microscope, and it is defined as:

$$\chi(\nu) = \pi \cdot \lambda(\Delta f \cdot \nu^2 - \tfrac{1}{2} C_s \cdot \lambda^2 \cdot \nu^4) \quad \textbf{(3)}$$

Where $C_s$ is the spherical aberration caused by the imperfections of the magnetic lenses, $\Delta f$ is the beam defocus (positive for underfocus) and $\lambda$ is the wavelength of the electrons in the beam. The main limitations imposed on the maximum achievable resolution with cryoTEM are mostly due to imperfections of the equipment. Especially the spherical aberration of the objective lens limits the obtainable resolution, which can be theoretically estimated by a formula (Wade, 1992):

$$d = (C_s \cdot \lambda^3)^{1/4} \quad \textbf{(4)}$$

Where $d$ is the maximum achievable resolution with an instrument with a spherical lens aberration of $C_s$ and electron wavelength of $\lambda$.

CryoTEM images are generally collected with settings where focus is set slightly under the image plane, instead of focusing on the image plane. This is done to enhance the phase contrast term, which arises from constructive interference. Because of the spherical aberration in the objective lens, an effect much like defocus is introduced and as a result the full beam is never focused at the focal plane at the same time (Erickson and Klug, 1971). The effect due to spherical aberration is partially compensated for by setting the focal level slightly underfocus, which enhances the phase contrast signal of features in a certain size range. This leads to the situation where the signal originating from features of a certain size is enhanced while the signal from features of different size is decreased. To observe features of all sizes in one image, several images collected at different defoci must be combined or alternatively a phase plate must be used.

Furthermore, as the phase contrast is a periodic sin function, half of the terms are negative; this can be corrected by flipping the negative terms to positive. To flip the phases, the defocus of the micrograph must first be determined, so that the CTF can be solved and phase amplitudes correctly flipped. Plotting of the CTF curve is useful for evaluation of the quality of the data. The presence of crystalline ice is easily detected by eye, but detection of drift and astigmatism is significantly more effective from the CTF curve. Additionally, comparison of the

CTF extracted from experimental data and the CTF calculated at the same defocus level gives a quick way to assess the degree of high resolution information present in the collected data (Angert et al., 2000; Mindell and Grigorieff, 2003).

A major obstacle for imaging vitrified biological samples with cryoTEM is the poor contrast. The interactions between electrons and sample depend on the atomic mass of the atoms in the sample. Water and proteins have two elements in common, oxygen and hydrogen. The non-shared elements, carbon, sulphur and nitrogen, have atomic masses very similar to that of oxygen. Thus, water interacts with electrons much like proteins and as such, proteins embedded in water produce minimal contrast. However, the use of water is essential as the use of alternative media potentially compromises the integrity of the protein structure.

The image formed in the electron microscope can be observed with a fluorescent screen or recorded either on electron sensitive film or with a specialized charge-coupled device (CCD) camera. The images recorded on film are then digitized with a scanner whereas the CCD-camera produces the digitized image directly. When the digitized image is immediately available, quality control can be conducted in real-time and problems in imaging conditions can be more readily detected. However, most CCD-devices are required to convert the electrons to photons which are then passed on and detected by the CCD-matrix. This process deteriorates the image quality as the incoming electrons and the phosphorous emitted photons spread laterally along the phosphor layer (Daberkow et al., 1991; Downing and Hendrickson, 1999). The correct thickness of the phosphor layer is critical, as although a thicker phosphor layer allows for maximal light output, it results in reduced spatial resolution (Faruqi and Tyrell, 1999). Additionally, the optimal phosphor layer thickness is dependent on the acceleration voltage used. The degradation due to lateral spread of electron and photons causes severe widening of the point spread function (PSF) from the theoretically-derived values (Faruqi and Andrews, 1997). Compensating measures, such as higher magnification, are required to match the resolution obtained by imaging on film (Faruqi and Subramaniam, 2000). Additionally, increasing the acceleration voltage leads to a decline of the high resolution information in the modulation transfer function (Downing and Hendrickson, 1999). However, the current generation of CCD-cameras already in use, have been shown to produce data of comparable quality to film (Booth et al., 2004; Saban et al., 2006; Zhang et al., 2003). Further improvements can be expected when CCD matrices capable of direct electron detection

become widely available (Faruqi, 2009; Faruqi and Henderson, 2007; McMullan et al., 2009).

## 1.4. Orientation search and three-dimensional reconstruction

In transmission electron microscope the final image is observed with a fluorescent plate, film or two-dimensional CCD-matrix and as such the outcome is a two dimensional image of a three-dimensional object. The situation is similar to a medical X-ray of human body. The information, or the shapes and sizes of all the organs, is compressed into a two-dimensional image, and it takes a trained person to interpret what the image tells about the state of the patient. To obtain a three-dimensional model of the patient something similar to magnetic resonance imaging (MRI) is required. In MRI the camera is rotated around the patient and projections of the patient are recorded. These projections are then mathematically combined to produce a three-dimensional model of the patient, which is then analyzed.

Similarly, the object observed in the TEM is three-dimensional, but what we see is only the projection of the object. The projection of the object depends on the orientation of the object in relation to the illuminating electron flux. Assuming that projections of the object in various orientations are available and the orientations are known, a three-dimensional reconstruction of the object can be completed. Unlike MRI, the three-dimensional image reconstruction of viruses relies on the notion that the particles are identical to each other and that they are suspended in random orientations in the vitreous water. These conditions allow collection of projections, representing the same object in various orientations. However, no information on the orientations is provided.

Thus, determination of the orientations of the particles becomes the key issue and several alternatives to accomplish this task are available. The initial model can be obtained from the raw data with the common lines method or the random model method. The common lines method searches for identical lines from the Fourier transforms of the 2D-projections (Fuller et al., 1996). For icosahedrally-symmetric particles this method is particularly powerful, as the symmetry gives rise to 37 pairs of lines per particle. Random model generation does not even attempt to assign correct orientations to particles, but assumes the centre of the particle is in the center of the box and assigns random orientations to a small subset of the particles, calculates a

three-dimensional reconstruction and refines the orientations of the subset against the model (Yan et al., 2007). Further orientation assignment, using the full dataset, is then performed using the subset model as an initial model. Alternatively, an object of the correct size and shape may be used as the initial model; even an idealized geometric construction can work (Baker and Cheng, 1996). For refinement of the orientations all the methods use an iterative approach, where projections of the model generated are used in the next iteration to improve the orientations of each particle.

This reasoning is valid, because the Fourier transforms of two-dimensional projections of a three-dimensional object are equivalent to the central cross-sections of the Fourier transform of the three-dimensional object (Crowther, 1971a). Thus, projections of the model can be correlated with the projections obtained via cryoTEM and with the real object. In addition to determining the orientations of each particle, it is necessary to fill the three-dimensional Fourier space, with the two-dimensional projections sufficiently, before an inverse three-dimensional transform can be calculated to a given resolution (Crowther, 1971a).

## 1.5. Cryo electron tomography

In many cases the individual viral particles are not identical, but pleomorphic human immunodeficiency virus 1 (HIV1) is an example of such a virus (Briggs et al., 2003). In this sort of situation the information for the three-dimensional reconstruction must be obtained from many views of just one particle. Cryo electron tomography (cryoET) is used to obtain three-dimensional structural information from one individual particle. This is achieved by tilting the sample in electron microscope and collecting several projections from the same area of the sample at different tilt angles (Figure 7). The tilt range of the specimen holder is usually limited to the range between -70° and +70° and the typical tilt angle step size is between 1.5° and 5° (Grünewald et al., 2003; Steven and Aebi, 2003). The number of projections that can be collected typically varies between 80 and 120 projections (Grünewald et al., 2003). Often the limiting factor for the number of projections that can be collected is the accumulating electron dose on the sample. The specimen can also be tilted around two axes, which allows more views of the object of interest to be collected (Penczek et al., 1995). To study one particle in the sample a three-dimensional tomogram, combining the information from

each projection and the initial tilt angles from the microscope, can be calculated and the area of interest can be isolated. The tomogram calculation requires accurate positioning of the projections in relation to each other and for this refinement of the tilt angles is required for instance, through the use of fiducial markers added to the specimen prior to vitrification (Castano-Diez et al., 2007; Kobayashi et al., 2009; Masich et al., 2006). Gold markers are commonly used since they have a very high contrast in the cryoTEM image.

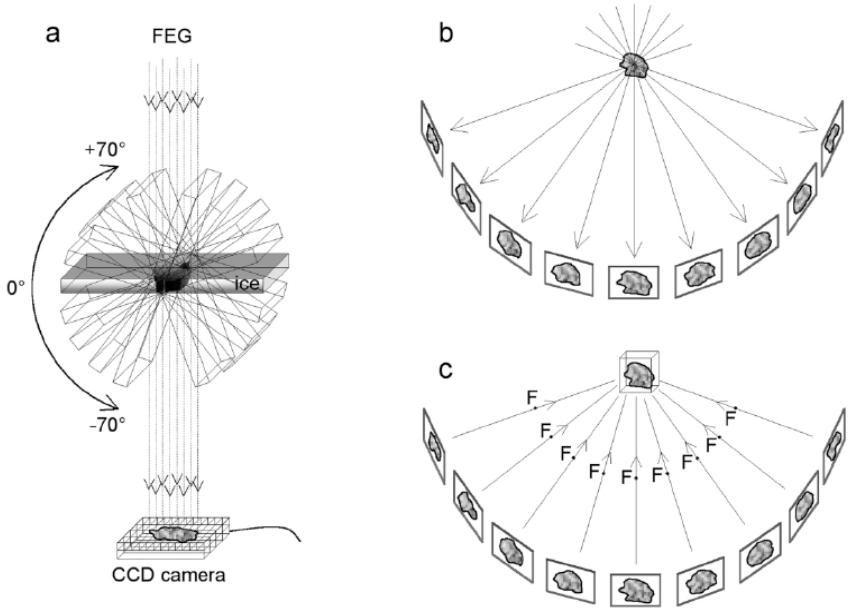


**Figure 7. Principle of electron tomography. The idea is to record series of 2D transmission electron micrographs at different tilt angles for individual 3D objects. In practice (a), the specimen holder is tilted incrementally around an axis perpendicular to the electron beam and projection images of the same specimen area are recorded at each position. A more schematic diagram (b) illustrates the images projected by a specimen at successive tilt angles. After mutual aligning all of these projection images, they are synthesized into a density map (the tomogram) by a weighted backprojection procedure (c), effected in Fourier space. This map represents the distribution of density through the specimen volume. Reprinted from (Grünewald et al., 2003) with permission from Elsevier.**

Single particle reconstructions have achieved resolutions around 3-4 Å, which is sufficient to track the carbon backbone and assign side chains to proteins, whereas the resolution achieved with cryoET is estimated to be around 5 to 8 nm(Grünewald et al., 2003; Masich et al., 2006). This is due to the insufficient number of views and views from high tilt ranges that are missing completely. Tighter spacing of the tilt step is impossible, as the accumulation of the electron dose

destroys the sample. Furthermore, increase of the sample thickness at the high tilt range adds noise to the collected data and weakens the contrast. CryoET is not capable of studying the fine details of biological macromolecules, but it is the only technique capable of three-dimensional studies of pleomorphic structures.

## 1.6. Homology modeling

Homology modeling refers to a method that uses the amino acid sequence to predict the structure of the protein. Typically the amino acid sequence is aligned to sequences that have known structures. The conserved regions are assigned secondary structure based on the known structures and the unconserved segments of the amino acid sequence are modeled computationally from scratch (Zhang, 2008). The final models are built by joining the domains. This type of homology modeling is referred to as “threading”. Unlike homology modeling where the entire sequence is matched to a single existing structure, the threading approach requires the match of the secondary structure features to existing templates. This is advantageous when no single close homolog of the query protein has a known structure. However, the threading approach will fail, if no suitable templates for the secondary structure prediction exist in the fold library. Additionally, the threading approach does not provide an actual model, but predicts an essentially correct fold for the query protein. The quality of homology model predictions depends heavily on the availability of suitable templates. If close homolog templates are available, high resolution models (RMSD 1-2 Å) can be readily achieved (Roy et al., 2010). Medium resolution models (RMSD 2-5 Å) can be achieved even with distant homolog models through the use of threading (Roy et al., 2010). The energy landscape hypothesis of protein folding predicts that the native state of a protein is also the energy minimum. Thus, the reliability of protein homology models is often estimated by evaluating the energy state of the models. The use of information derived from known structures is necessary, as proteins typically contain too many atoms for calculation of predictions that are based solely on interactions between the atoms.

## 2. Materials and methods specific to studies included this thesis

BRV was purified from inoculated and systematically infected *Chenopodium quinoa* Willd. plants. Polyclonal antisera against the C-terminal peptides of denatured BRV capsid protein were generated in rabbits. The binding of the antibodies to denatured BRV capsid protein was observed by western blotting. The details are as described in study I.

HPEV1 was cultured in a human lung carcinoma cell line and purified as described earlier (Abraham and Colonno, 1984). Integrin $\alpha_V\beta_6$ ectodomain was expressed in CHO cells and purified as described earlier (Weinacker et al., 1994; Williams et al., 2004). Integrin $\alpha_V\beta_3$ was obtained commercially (BioMarket Ltd., Finland) and Triton X-100 was removed prior to biochemical assays. Binding of integrins $\alpha_V\beta_3$ and $\alpha_V\beta_6$ to HPEV1 was analyzed in a solid-phase integrin binding assay. The ability of integrins $\alpha_V\beta_3$ and $\alpha_V\beta_6$ to prevent HPEV1 plaque formation was analyzed in a plaque neutralization assay. To test whether or not small RGD peptides can block the binding of integrins $\alpha_V\beta_3$ and $\alpha_V\beta_6$ to HPEV1, a peptide blocking assay was performed. These steps are described in study II.

CAV7 was propagated in B-Vero cells and purified in CsCl gradients. To analyze the stability of CAV7 particles, virus preparations were heated to 56°C for 30 min immediately prior to vitrification (Hewat and Blaas, 2004). The stability of native CAV7 particles was also tested by comparing the infectivity of CAV7 stored at -80 °C versus freshly-prepared CAV7, in two different sample buffers. Two CAV7 strains from laboratory collections were separately grown and purified. The viruses were identified as CAV7 strains by CAV7-specific antiserum and viral RNA was extracted. RT-PCR was performed and the 3 kb amplicon was subjected to stepwise sequencing using primers that were generated according to CAV7-Parker. The details involved in these steps are described in study III.

Low dose EM data for all projects were collected with a FEI Tecnai F20 microscope operated at 200kV. The spherical aberration of the instrument is 2.0 mm. The icosahedral reconstruction data in all studies were recorded on Kodak SO163 film with a 62000× magnification. The micrographs were scanned with a Zeiss PhotoScan TD scanner with a step size of 7 µm. The tomographic data in study II were recorded with a

Gatan UltraScan 4000 CCD camera with 39400× and 48000× magnifications, using SerialEM software (Mastronarde, 2005). The pixel size in the CCD cell used was 15 µm.

For the icosahedral reconstruction data the contrast transfer function was estimated with CTFFIND3 (Mindell and Grigorieff, 2003). The particles were picked automatically with a program named ETHAN (Kivioja et al., 2000) and manually checked and extracted using EMAN (Ludtke et al., 1999). The reconstructions were done either with a combination of PFT2 (Baker and Cheng, 1996), POR (Ji et al., 2006) and EM3DR2 (Marinescu and Ji, 2003) (Study I) or with AUTO3DEM (Yan et al., 2007) (Studies II and III). In study II a bfactor correction was applied through the AUTO3DEM system. In study III the bfactor was estimated and corrected with EM-Bfactor (Fernandez et al., 2008; Rosenthal and Henderson, 2003). The homology modeling of the BRV capsid protein (Study I) and CAV7 capsid proteins (Study III) was carried out with I-TASSER (Zhang, 2009). The homology modeling of the $\beta_6$ subunit of integrin $\alpha_V\beta_6$ (Study II) was carried out with Phyre (Kelley and Sternberg, 2009). The tomographic reconstructions were calculated and visualized with IMOD (Kremer et al., 1996). All other visualizations were done with UCSF Chimera (Pettersen et al., 2004).

# D. RESULTS AND DISCUSSION

We solved the structures of the selected viruses BRV (Study I), HPEV1 (Study II) and CAV7 (Study III). In addition we solved the structure of CAV7 empty capsid (Study III) and the structure of HPEV1 complexed with integrins $\alpha_V\beta_3$ and $\alpha_V\beta_6$ (Study II). As all of the viruses studied exhibit icosahedral symmetry, the method of choice for all projects was model-based icosahedral three-dimensional reconstruction, which allows full exploitation of the high symmetry found in icosahedral capsids. To observe the number and conformation of integrin molecules bound to HPEV1 we performed tomography (Study II). Antibodies against the C-terminus of BRV capsid protein were used to determine if the shorter form of the capsid protein is a truncated form of the larger form (Study I). The effect of soluble integrins $\alpha_V\beta_3$ and $\alpha_V\beta_6$ to HPEV1 infection was studied with a plaque neutralization assay (Study II). Furthermore, the ability of RGD-peptides to block the interaction between integrins $\alpha_V\beta_3$ and $\alpha_V\beta_6$, and HPEV1 was studied with peptide-blocking assay (Study II). To compare genomic differences and to generate a homology models of the USSR and the 275/58 strains of CAV7, the RNA genome of USSR and 275/58 strains of CAV7 were sequenced (Study III). Homology models of the capsid protein of BRV (Study I), capsid proteins VP1, VP2 and VP3 of CAV7 (Study III) and the β-subunit of integrin $\alpha_V\beta_6$ were generated (Study II). The homology modeled capsid protein of BRV was aligned to that of the TRSV X-ray model (Study I) and the homology modeled capsid proteins of CAV7 were fitted into the corresponding segmented densities of CAV7 capsid proteins (Study III) using the rigid body fitting algorithm embedded in UCSF Chimera (Pettersen et al., 2004). Additionally, the aligned homology model of BRV capsid protein was used to generate the whole capsid of BRV (Study I) using the Oligomer Generator in ViperDB (Shepherd et al., 2006).

# 1. The structure of the BRV capsid

## 1.1. The cryoEM reconstruction

We solved the structure of the native BRV capsid to 17 Å resolution using cryoEM and icosahedral image reconstruction techniques (Study I; Figure 1b). Sections of the capsid revealed icosahedrally organized RNA density inside the capsid (Study I; Figure 1c and 1d). Amino acid sequence comparisons of the structural protein revealed the closest relative of BRV that had a structure available was TRSV (Study I; Figure 2). Comparisons between the cryoEM reconstruction of the BRV capsid and the X-ray model of TRSV revealed the structures to be nearly identical (Study I; Figure 3a and 3b). Using difference imaging between the cryoEM reconstruction of BRV and the X-ray model of TRSV filtered to 17 Å resolution we managed to differentiate the densities deriving from protein and RNA. With the results from the difference imaging we could determine that the RNA density followed the contours on the inside of the protein shell closely, filling the protrusions at the five-fold axes (Study I; Figure 1e and 1f).

## 1.2. Homology modeling

Once the structural similarity had been confirmed we proceeded to produce a highly reliable homology model of the BRV capsid protein. The carbon backbone trace of the homology modeled capsid protein was very similar to that of the TRSV X-ray structure (Study I; Figure 3a and 3b). The BRV capsid protein homology model was aligned to that of the TRSV X-ray model and then used to generate the whole capsid of BRV (Study I; Figure 3c and 3d). Amino acid sequence comparison of nepovirus capsid proteins revealed, that BRV has a three amino acid insertion (KAG) in the DE loop (Study I; Figure 2). Using the full capsid homology model we looked for the position of the loop indicated in the amino acid sequence comparison. The DE loop was found on the surface of the capsid, clustering near the five-fold axes (Study I; Figure 3c and 3d). The importance of a specific coat protein sequence in insect transmission has been demonstrated (Atreya et al., 1991). The clustering of the DE loop in BRV may enhance vector-virus interaction and supports the hypothesis that this loop may have a

role in the mite-transmission. The residues involved in the protein-RNA contacts were studied by fitting the homology model of the BRV in the cryoEM density of the BRV (Study I; Figure 3e). The fit placed residues 1-3 (SGL), 112-114 (TFT) and 290-292 (FHI) closest to the protein-RNA interaction sites. The importance of protein-RNA interactions in virus capsid assembly have been well characterized in MS2 (Morton et al., 2010; Rolfsson et al., 2010; Toropova et al., 2008). The viral protein-RNA interactions have not been conclusively shown to be important in the uncoating of picornavirus superfamily members, but the capsid proteins VP1 and VP4 have been suggested to be functionally involved in PV1 uncoating and the protein-RNA interactions may have a role in uncoating (Danthi et al., 2003). Thus the protein-RNA interactions identified in BRV (Study I) may indicate important sites for capsid assembly and uncoating, and the predicted residues provide potential targets for studying these processes in BRV.

### 1.3. Short form of the capsid protein

Western blot of capsid proteins incubated with antibodies specific to the C-terminus of the BRV capsid protein revealed that only the longer form of the capsid protein binds the very C-terminal antibody (Study I; Figure 4). Thus, we concluded that the shorter form of the capsid protein is due to a C-terminal truncation of the longer form. The truncation may arise either during infection or the purification process, but the exact reason for the truncation remains unclear.

## 2. The structure of the HPEV1 capsid

### 2.1. The cryoEM reconstruction of the HPEV1 capsid

We solved the structure of HPEV1 native capsid to 8.5 Å resolution (Study II; Figure 2E and 3). Amino acid sequence comparison of VP1 to other picornaviruses revealed little similarity (Study II; Figure 1). Comparison of the structure to other known picornavirus structures filtered to 8.5 Å resolution confirmed that HPEV1 structure differs significantly from other known structures (Study II; Figure 3). The signature truncated five-fold vertex was found only in FMDV. Further examination of the amino acid sequence alignments revealed that both FMDV and HPEV1 have

deletions in the VP1 β-barrel surface exposed loops, which are responsible for forming the five-fold protrusions (Study II; Figure 1). One of the deletions is extensive enough to potentially merge the β-sheets of the VP1 β-barrel, leading to a seven sheet β-barrel, like in FMDV, instead of the more common eight sheet β-barrel found in other picornavirus structures (Acharya et al., 1989; Hendry et al., 1999; Hogle et al., 1985; Rossmann et al., 1985).

Furthermore, we observed a novel "finger-like" structure near the five-fold vertices, extending approximately 30 Å into the capsid (Study II; Figure 4C-E). The density of the fingers was markedly higher than the density of the capsid protein shell in the reconstruction (Study II; Figure 2E). The position of the fingers was compared to the position of CAV9 capsid proteins. The comparison placed the fingers very close to the position where the N-termini of CAV9 VP1 and VP4 lie, however the fingers extend further into the capsid (Study II; Figure 4C-E). We speculate that the fingers are a site of protein-RNA interaction, and as HPEV1 lacks the cleavage of VP0 to VP2 and VP4, we suspect that the N-termini of VP0 and VP1 are involved in the interaction. Additionally, the very high density of fingers suggests that the fingers are highly organized material, possibly highly-ordered duplex RNA and protein. The fingers potentially indicate positions which are important in capsid assembly, as has been shown for MS2, or RNA uncoating, as has been speculated for PV1 (Danthi et al., 2003; Morton et al., 2010; Rolfsson et al., 2010; Toropova et al., 2008). In assembly these areas may function as RNA binding sites in pre-assembled subunits, where RNA binding drives the assembly. Alternatively, the fingers may mark the position of a protein terminal or loop that is externalized during uncoating, pulling the RNA along and driving the uncoating. Both of these aspects would be interesting to study with mutation studies in the coat proteins at this region. The RNA genome could also be analyzed for the existence of energetically-favorable stem-loop structures that might be involved in assembly as is the case for MS2 (Horn et al., 2006; Morton et al., 2010; Valegård et al., 1997). Expression of the capsid proteins individually in a recombinant system could also prove helpful in assembly studies, as has been done for example with CCMV and MS2 (Fox et al., 1998; Valegård et al., 1997).

## 2.2. Integrin binding to HPEV1

An infectivity assay showed that, while incubation in the presence of soluble, recombinant, extracellular segment of integrin $\alpha_V\beta_6$ blocked HPEV1 infection, whereas incubation with soluble full length integrin $\alpha_V\beta_3$ rather enhanced than blocked the infection (Study II; Figure 5). The observed difference may be due to different forms of the integrins. Only the extracellular segment of integrin $\alpha_V\beta_6$ was used, whereas the full length integrin $\alpha_V\beta_3$ was used. A fraction of the full length integrin $\alpha_V\beta_3$ may have been incorporated to the cell membrane before or after binding to HPEV1 increasing the number of integrin molecules on the cell surface, thus increasing the infectivity. Alternatively, as the integrin $\alpha_V\beta_3$ was observed to aggregate efficiently at higher concentrations, it may be that the clustering of integrin $\alpha_V\beta_3$ molecules reduces the number of molecules able to bind HPEV1.

The interaction between full length integrin $\alpha_V\beta_3$ and recombinant, extracellular part of integrin $\alpha_V\beta_6$ was studied with peptide blocking assays. The assays showed that the RGD-motif is a major binding site for both integrins (Study II; Figure 5). Furthermore, my comparison of the β-subunit of integrin $\alpha_V\beta_3$ and the homology model of the β-subunit of integrin $\alpha_V\beta_6$ revealed limited conservation of the amino acid sequence in the region of the RGD binding site (unpublished data). Thus the difference in the affinity for RGD-peptides is most likely due to the differences in the β-subunit.

## 2.3. Reconstructions of HPEV1 complexed with integrins

The results of the binding assays led us to produce vitrified samples of HPEV1 complexed with either integrin $\alpha_V\beta_3$ or $\alpha_V\beta_6$ (Study II; Figure 2B and 2C). To optimize the complex sample for cryo preparation variable mixture ratios of HPEV1 and integrins were tested. Ratios ranging from one binding site per one integrin molecule to one binding site per 50 integrin molecules were tested. The optimal ratio was found to be three integrin molecules per two binding sites, for both integrins.

In the micrographs we observed only a few integrins bound per particle and in variable conformations. To further confirm the situation we performed cryo-electron tomography on the sample (Study II; Figure 2D). The

tomography confirmed that the degree of labeling varied from 1 to 6 integrin molecules bound per particle and the conformation of the integrin molecules varied significantly. The number of integrin molecules bound did not increase even when we prepared the sample with 50-fold excess of integrin per binding site. Furthermore, in the integrin $\alpha_V\beta_3$ complexed sample we observed a strong tendency of the integrin-complexed particles to form aggregates (unpublished data). The tendency is most likely due to the transmembrane domain, present in the commercial integrin $\alpha_V\beta_3$ sample. The $\alpha_V\beta_6$ protein was a recombinant ectodomain lacking the transmembrane sequence and was easier to work with. Statistical comparison of the ratio of empty capsids to full in virion and the virion with the integrins showed that there was no statistically significant indication of either integrin initiating uncoating of the HPEV1 under the conditions used (Study II; Table 1).

The structures of HPEV1 complexed with integrins $\alpha_V\beta_3$ and $\alpha_V\beta_6$ were solved to 15 Å and 8.7 Å resolutions, respectively (Study II; Figure 7A and 7B). The density of the integrin molecules was very weak in the reconstructions and the contact between HPEV1 and integrin $\alpha_V\beta_3$ was only visible when the viewing threshold was set below the mean density level. However, the observed low density of the integrin molecules is in line with the low occupancy of integrin molecules on the viral surface, as was observed in the tomographic data (Study II; Figure 2D). The contact points, residing between the three-fold and five-fold axes, were nearly identical for both integrins. Comparison with the X-ray model of CAV9 places the position of the integrin foot-print on residues 268-270 (PTP) of CAV9 VP1 (Study II; Figure 7C and 7D). The amino acid sequence alignment featured an approximately 20 amino acid deletion in the C-terminus of HPEV1 (Study II; Figure 1). When this deletion is taken into account, the position of the integrin footprint on the CAV9 X-ray structure matches fairly well with the predicted position of the RGD-motif in CAV9.

# 3. The structure of CAV7 capsid

## 3.1. Differences in the sequences of CAV7 strains

The USSR and 275/58 strains of CAV7 were sequenced and amino acid sequence comparisons of the revealed the capsid proteins of the USSR strain to be nearly identical with the Parker strain sequenced earlier (Study III; Supplementary material). The capsid proteins VP2 and VP4 of the USSR strain and the Parker strain were found to be identical and only a few point mutations in the amino acid sequences were observed in VP1 and VP3 (Study III; Supplementary material). Each of the 275/58 strain capsid proteins were found to contain several point mutations in comparison to the Parker strain capsid proteins (Study III; Supplementary material). However, as the pathogenesis of the 275/58 strain differs from both the USSR and the Parker strain, these point mutations are likely to be, at least partially, responsible for the observed differences.

## 3.2. The structure of CAV7 empty and filled capsid

We chose to solve the structure of CAV7 USSR strain and so we prepared vitrified samples from purified virus extract. Initial inspection of the micrographs revealed that the sample consisted of approximately one third RNA filled, capsids and two thirds empty capsids (Study III; Figure 1). We tried to investigate the source of the empty capsids in the preparation by studying the effect of pH, freezing and thawing, and buffer composition by infectivity measurement and observation by cryoEM (Study III; Table 1). The experiment demonstrated that neither the infectivity nor the percentage of empty particles was significantly affected by buffer composition or a freeze-thaw cycle. This result was not surprising since the ability to tolerate pH changes is typical for enteroviruses. We then used heat treatment to generate empty particles and analyzed the structure of capsids. Heat treatment of full CAV7 particles significantly reduced the infectivity (around 1,000-fold decrease). Additionally, no full particles were detected in cryoEM images of the heat treated CAV7 sample (Study III; Table 1).

The particles from mixed population micrographs were divided in to empty and filled datasets and processed independently. The empty capsids

from micrographs of the heat treated sample were initially processed independently to reveal possible differences to the empty capsid reconstruction from the mixed population sample. After the refinement had halted and no differences could be discerned, the empty capsid datasets were combined. Ultimately, the CAV7 filled and empty capsid structures were solved to 8.2 Å and 6.1 Å resolutions respectively (Study III; Figure 3A and 3B). Comparison of the maps revealed that the CAV7 filled capsid has an opening at the five-fold symmetry axis, whereas the CAV7 empty capsid is closed at the five-fold symmetry axis (Study III; Figure 3A and 3B). The capsid proteins VP1, VP2 and VP3 were manually segmented from both of the reconstructions (Study III; Figure 4A). Comparison between the capsid proteins derived from the empty capsid reconstruction and those derived from the filled capsid reconstruction revealed no apparent changes in VP2 or in VP3. However, in VP1 the comparison revealed a slight domain movement, which appears to determine the state of the opening at the five-fold vertex (Study III; Figure 4B).

The density for VP4 could not be detected by difference imaging, but putative density for the capsid protein VP4 was found in the full capsid reconstruction, near the five-fold vertex (Study III; Figure 3C). The density of the putative VP4 in the full capsid reconstruction was found to be similar to the density of the RNA. This is probably due to non-homogeneity in the dataset, as the some of the full capsids may have lost their VP4 while retaining their RNA, as happens with PV1 upon receptor binding (Arita et al., 1998). The segmented density of VP4 appears quite massive in comparison with the segmented density of the other, larger capsid proteins and thus it is very likely that it contains density belonging to either RNA or one of the other capsid proteins. The effect of the heating on CAV7 was confirmed by infectivity assay and cryoEM (Study III; Table 1). The micrographs of the heat treated sample had no filled capsids, whereas the untreated sample displayed the expected one third filled particles.

## 3.3. Homology models of the capsid proteins

As CAV7 amino acid sequence analysis revealed relatives that have X-ray structures available, thus we proceeded to attempt homology modeling of the capsid proteins (Study III; Supplementary material). Reliable models were then generated for capsid proteins VP1, VP2 and VP3 (C-scores: 0.60, 1.08 and 1.33, respectively). In I-TASSER, a model with a C-score above -1.5 is considered to have the

correct fold (Roy et al., 2010). The homology modeling of VP4 produced a less reliable model, but one that still has a C-score above the cut-off (C-score: -0.93). The homology modeled capsid proteins were fitted into the segmented density of CAV7 capsid proteins using a rigid body fitting algorithm (Study III; Figure 4A). Majority of the homology models fit in the corresponding segmented density. Especially the strands that make up the β-barrels fit well with the segmented density. However, as the intertwining parts of the capsid proteins could not be separated from each other by segmentation, the correctness of the homology predictions remains partially unconfirmed.

The point mutations in the USSR and 275/58 strains were mapped on the respective homology modeled capsids (Study III; Figure 5). The mapping revealed many surface exposed residues in the 275/58 strain, while in the USSR strain only a few surface exposed residues were observed. Interestingly, one of the surface exposed point mutations in the 275/58 strain occurs directly at a site homologous to the receptor binding sites in PV1, CAV21 and CBV3 (He et al., 2000; He et al., 2001; Xiao et al., 2005a). Furthermore, four additional point mutations cluster near the same site. It is conceivable, that these point mutations affect the receptor binding of the 275/58 strain and thus are responsible for the altered virulence of the 275/58 strain.

The CAV7 structure is from a taxonomic group that has had no structural information available before. The fitting of the homology models of the capsid protein could be improved by applying flexible fitting. When combined with the homology model predictions it becomes possible to generate a road map of the surface exposed amino acid residues.

# E. CONCLUSIONS AND FUTURE STUDIES

Although the three projects described in this thesis were carried out independently, there are several points that one can draw only when considering them as a whole. In the following section I will summarize these. The three different picornaviruses studied showed the huge advantages that can be gained only through the combination of experimental structure determination with homology modeling and biochemical studies. It was possible to very reliably predict some capsid protein tertiary structures as expected given the large number of picornavirus-like atomic models available in the Protein Data Bank. However, due to the very diverse nature of these deceptively simple viruses due to evolutionary pressures brought about by interactions with their respective hosts, this simple β-barrel framework has such variation and elaborations on it that the exact side-chain interactions, and even the fold of some of the proteins, for example the capsid proteins of HPEV1 (Study II) , could not be predicted using the best currently-available threading algorithms used by Phyre and I-TASSER (Kelley and Sternberg, 2009; Roy et al., 2010). Hence the structural verification, even at the limited resolutions achieved in this study, are informative.

Despite the significant variance found in the amino acid sequences of icosahedral members of the picornavirus superfamily, the β-barrel fold of the structural proteins is well conserved. Interestingly, the fold is conserved between members of the supergroup regardless of whether the host cell is a plant cell or an animal cell. However, the currently available results suggest that the animal and plant viruses differ in the cleavage of the β-barrel domains of the capsid proteins, which are cleaved nearly always in the animal viruses, but rarely in plant viruses. This could be an adaptation to facilitate more efficient exploitation of the intake mechanisms found in animal cells and manipulation of the plasma membrane. Whilst the β-barrel fold is well conserved, the primary amino acid sequence undergoes rapid changes, as has been observed with, for example EV71 (van der Sanden et al., 2010). The conservation of the β-barrel fold extends beyond the picornavirus superfamily and the β-barrel fold has been observed in members of many virus families, including RNA and DNA viruses from all domains of life (Nandhagopal et al., 2002). Additionally, viral lineages have been organized based on the conservation of structure, as structure is preserved more strictly

than amino acid sequence. The β-barrel domain is a versatile building block for viral capsids as it requires no specific orientation in the capsid, for example the β-strands of the β-barrel domains are found to be roughly perpendicular to the capsid surface in e.g. adenoviruses and parallel in e.g. tomato bushy stunt virus (Harrison et al., 1978; Roberts et al., 1986).

Prediction of virus-host interactions from sequence data alone is nearly impossible. The use of high reliability homology modeling helps in these pursuits by providing indications of amino acid residues that are surface exposed, but prediction of specific interactions remains extremely difficult. On the other hand, structural studies can be used to produce reliable evidence of the virus-host interactions and homology modeling can be combined with the results of the structural studies to enhance the interpretation, as has been seen for example with herpes simplex virus (Baker et al., 2003; Bowman et al., 2003; Lasker et al., 2009; Topf et al., 2006; Topf et al., 2008). In this study the combination of structural studies and homology modeling enabled the prediction of surface exposed residues, as well as residues involved in protein-RNA interactions. Even with highly reliable homology models and high resolution structures, such predictions should be tested and verified with mutational studies.

Electron cryo-microscopy and image reconstruction is a relatively young field that is still advancing quickly. The development of instruments and techniques has had a huge impact on the results achieved with cryoEM and image reconstruction, even within the short time span of this project as seen in the results presented here. The software used for the orientation search in studies II and III (AUTO3DEM) resulted in a significant improvement of resolution in comparison to study I (PFT2 and POR) (Baker and Cheng, 1996; Ji et al., 2006; Yan et al., 2007). The increased efficiency of calculations allowed more freedom for optimization of the iteration conditions and the data could be exhaustively iterated in a reasonable time. For fine refinement the use of larger datasets improved signal to noise ratio, which enabled higher resolution reconstructions. The use of advanced graphics, including stereo graphics, for the analysis of the higher resolution reconstructions aided greatly the interpretation of the results. The data in these studies were mainly limited by the sample preparation and the electron microscope used which has a relatively unstable side entry stage and a low operating voltage. Although, to the best of my knowledge, 6Å in a virus reconstruction for this design is the highest resolution that has been reported (Study III). To date the highest resolutions reached with

cryoEM and icosahedral image reconstruction techniques are between 3-4 Å (Chen et al., 2009; Liu et al., 2010; Yu et al., 2008; Zhang et al., 2010; Zhang et al., 2008b). To calculate a very high resolution reconstruction, the quality and the consistency of the data becomes critical. Even though electron microscopes of older design allow the collection of high resolution data, the lack of stability results in great variance in the quality of the data collected and accumulation of a large dataset of high quality becomes very tedious. The newer electron microscopes operating at higher voltages with better pole piece designs have the advantage that they are stable enough to allow collection of high quality data more on regular basis and thus enable the collection of huge datasets of high quality (Zhang et al., 2010; Zhang et al., 2008b).

Contacts between the capsid proteins and RNA were observed in every virus studied, this is due to collecting the low resolution information that tells about the RNA density, albeit inappropriately averaged, which is ignored in x-ray processing as low resolution information is not generally collected or modeled. The protein-RNA contacts are likely to play a part in the capsid assembly and possibly in the uncoating event as well. Studies on MS2 indicate that protein-RNA interactions are very important for capsid assembly and anti-viral agents, inhibiting the interaction between viral proteins and viral RNA, have been suggested (Morton et al., 2010). Such anti-virals could also prove effective against the members of the picornavirus superfamily.

An alternative strategy that emerges from these studies is the identification of surface epitopes involved in host-cell interactions. One could investigate the use of peptides mimicking these epitopes as antiviral agents disrupting the initial stages of entry. One example could be the putative mite-transmission epitopes of BRV that may offer a low-cost method to prevent transmission of BRV from plant to plant. This should be pursued further as success might provide economic advantages and an approach which could be generalized for other pathogens of cultivated plants. It would also be interesting to perform a mutagenesis study on one of the CAV7 strains to determine which, if any, of the observed point mutations can explain the altered pathogenesis of the CAV7 275/58 strain. Additionally, comparison of the structural road maps between CAV7 and related viruses, whose crystal structure are known, could be used to detect areas similar to known receptor binding sites and thus aid in the search for CAV7 receptors.

The receptor binding studies on HPEV1 revealed two receptors of HPEV1, integrin $\alpha_V\beta_3$ and integrin $\alpha_V\beta_6$. However, neither of the receptors indicated ability to initiate

the uncoating of the HPEV1 genome and currently it seems that both of the receptors are primarily attachment receptors. The role of the integrin receptors in HPEV1 cell entry requires further studies and possibly more receptors need to be identified by siRNA screening for example. The existence of additional receptors is probable as other HPEV serotypes have been identified that lack the RGD motif, and these could then be used in comparison studies to help in mapping out the first stages of HPEV cell entry.

Although many of the picornaviruses can cause central nervous system (CNS) related symptoms it is worth noting that only a few of them have been reported to cause paralytic symptoms. It would be most interesting to study why the infection by for example poliovirus, CAV7 or EV71 can cause paralysis, whereas others like for example, HPEV1 do not. Are there perhaps some subtle differences in replication or release in neural cells that are the reason for this difference in pathogenicity? This matter is worth further studies to gain insight on the mechanisms of picornaviruses. Structural studies can help with these goals by providing molecular details on virus-receptor interaction, structural changes involved in cell entry, and amino acid residues critical for successful infection.

# F. ACKNOWLEDGEMENTS

The work presented in this thesis was carried out in the Finnish Academy Centre of Excellence in Virus Research 2006-2011, at the Institute of Biotechnology and Department of Biosciences, Faculty of Biological and Environmental Sciences, University of Helsinki, under the supervision of Dr Sarah Butcher.

First and foremost I must express my gratitude to my supervisor Dr Sarah Butcher. She took me in as a master's student and introduced me to cryoEM. It is no exaggeration to say that this thesis would not exist without her guidance and motivation. Sarah has always managed to offer a pleasant work environment where I have had the freedom to work on my projects in the manner that suits me best and whenever I needed advice she has always found the time to discuss no matter how busy she was.

Many thanks also go out to our collaborators in Turku Dr Timo Hyypiä, Dr Petri Susi, Outi Heikkinen and Ritva Kajander for providing us with the samples to image and also for all the discussions we had over the years.

I also thank Dr Jari Valkonen and Dr Pirkko Heikinheimo for reviewing and improving my thesis.

I am also very grateful for the guidance I received from Dr Juha Huiskonen, Dr Harri Jäälinoja, Pasi Laurinmäki and Benita Koli. They are the ones who I learned most of the practical aspects of cryoEM and image processing from. In addition Pasi has helped me tremendously with the data collection and he has been a frequent company on my sample preparation trips to Turku, making the travelling much more pleasant.

I would also like to thank my current co-workers Lotta Happonen, Violeta Manole, Lassi Liljeroos, Katarina Hattula and Ari Ora for adding to the pleasant atmosphere that we have in the group and also for tolerating and answering my silly questions about biology.

My thanks also go to the people who manage The National Doctoral Programme in Informational and Structural Biology. More specifically, I thank Mark Johnson and Fredrik Karlsson for the winter school events they organized annually.

I thank all my teachers who have guided me thus far. Specifically I must thank Arto Annila for guiding me to Sarah's door when I was starting my master's thesis.

I thank my parents for their continued support over the years.

I thank my family for the support and understanding they have shown me, and for keeping me busy outside of work.

# G. REFERENCES

**Abraham, G., and Colonno, R.J. (1984). Many rhinovirus serotypes share the same cellular receptor. J Virol *51*, 340-345.**

**Acharya, R., Fry, E., Stuart, D., Fox, G., Rowlands, D., and Brown, F. (1989). The three-dimensional structure of foot-and-mouth disease virus at 2.9 A resolution. Nature *337*, 709-716.**

**Adrian, M., Dubochet, J., Lepault, J., and McDowall, A.W. (1984). Cryo-electron microscopy of viruses. Nature (London) *308*, 32-36.**

**Ang, L.W., Koh, B.K., Chan, K.P., Chua, L.T., James, L., and Goh, K.T. (2009). Epidemiology and control of hand, foot and mouth disease in Singapore, 2001-2007. Ann Acad Med Singapore *38*, 106-112.**

**Angert, I., Majorovits, E., and Schröder, R.R. (2000). Zero-loss image formation and modified contrast transfer theory in EFTEM. Ultramicroscopy *81*, 203-222.**

**Ansardi, D.C., Luo, M., and Morrow, C.D. (1994). Mutations in the poliovirus P1 capsid precursor at arginine residues VP4-ARG34, VP3-ARG223, and VP1-ARG129 affect virus assembly and encapsidation of genomic RNA. Virology *199*, 20-34.**

**Arita, M., Koike, S., Aoki, J., Horie, H., and Nomoto, A. (1998). Interaction of poliovirus with its purified receptor and conformational alteration in the virion. J Virol *72*, 3578-3586.**

**Arita, M., Nagata, N., Iwata, N., Ami, Y., Suzaki, Y., Mizuta, K., Iwasaki, T., Sata, T., Wakita, T., and Shimizu, H. (2007). An attenuated strain of enterovirus 71 belonging to genotype a showed a broad spectrum of antigenicity with attenuated neurovirulence in cynomolgus monkeys. J Virol *81*, 9386-9395.**

**Arita, M., Shimizu, H., Nagata, N., Ami, Y., Suzaki, Y., Sata, T., Iwasaki, T., and Miyamura, T. (2005). Temperature-sensitive mutants of enterovirus 71 show attenuation in cynomolgus monkeys. J Gen Virol *86*, 1391-1401.**

**Atreya, P.L., Atreya, C.D., and Pirone, T.P. (1991). Amino acid substitutions in the coat protein result in loss of insect transmissibility of a plant virus. Proc Natl Acad Sci U S A *88*, 7887-7891.**

**Baker, M.L., Jiang, W., Bowman, B.R., Zhou, Z.H., Quiocho, F.A., Rixon, F.J., and Chiu, W. (2003). Architecture of the herpes simplex virus major capsid protein derived from structural bioinformatics. J Mol Biol *331*, 447-456.**

**Baker, T.S., and Cheng, R.H. (1996). A model-based approach for determining orientations of biological macromolecules imaged by cryoelectron microscopy. J Struct Biol *116*, 120-130.**

**Baker, T.S., Olson, N.H., and Fuller, S.D. (1999). Adding the third dimension to virus life cycles: three-dimensional reconstruction of icosahedral viruses from cryo-electron micrographs. Microbiol Mol Biol Rev *63*, 862-922.**

**Baker, T.S., Olson, N.H., and Fuller, S.D. (2000). Adding the third dimension to virus life cycles: three-dimensional reconstruction of icosahedral viruses**

**from cryo-electron micrographs. Microbiol Mol Biol Rev *64*, 237-237.**

**Bamford, D.H., Grimes, J.M., and Stuart, D.I. (2005). What does structure tell us about virus evolution? Curr Opin Struct Biol *15*, 655-663.**

**Basavappa, R., Syed, R., Flore, O., Icenogle, J.P., Filman, D.J., and Hogle, J.M. (1994). Role and mechanism of the maturation cleavage of VP0 in poliovirus assembly: structure of the empty capsid assembly intermediate at 2.9 A resolution. Protein Sci *3*, 1651-1669.**

**Basnak, G., Morton, V.L., Rolfsson, O., Stonehouse, N.J., Ashcroft, A.E., and Stockley, P.G. (2010). Viral genomic single-stranded RNA directs the pathway toward a T=3 capsid. J Mol Biol *395*, 924-936.**

**Bayer, N., Prchla, E., Schwab, M., Blaas, D., and Fuchs, R. (1999). Human rhinovirus HRV14 uncoats from early endosomes in the presence of bafilomycin. FEBS Lett *463*, 175-178.**

**Bedard, K.M., and Semler, B.L. (2004). Regulation of picornavirus gene expression. Microbes Infect *6*, 702-713.**

**Blomqvist, S., Paananen, A., Savolainen-Kopra, C., Hovi, T., and Roivainen, M. (2008). Eight years of experience with molecular identification of human enteroviruses. J Clin Microbiol *46*, 2410-2413.**

**Boonyakiat, Y., Hughes, P.J., Ghazi, F., and Stanway, G. (2001). Arginine-glycine-aspartic acid motif is critical for human parechovirus 1 entry. J Virol *75*, 10000-10004.**

**Booth, C.R., Jiang, W., Baker, M.L., Zhou, Z.H., Ludtke, S.J., and Chiu, W. (2004). A 9 angstroms single particle reconstruction from CCD captured images on a 200 kV electron cryomicroscope. J Struct Biol *147*, 116-127.**

**Bowman, B.R., Baker, M.L., Rixon, F.J., Chiu, W., and Quiocho, F.A. (2003). Structure of the herpesvirus major capsid protein. EMBO J *22*, 757-765.**

**Brault, V., Uzest, M., Monsion, B., Jacquot, E., and Blanc, S. (2010). Aphids as transport devices for plant viruses. C R Biol *333*, 524-538.**

**Briani, F., Deho, G., Forti, F., and Ghisotti, D. (2001). The plasmid status of satellite bacteriophage P4. Plasmid *45*, 1-17.**

**Briggs, J.A., Wilk, T., Welker, R., Krausslich, H.G., and Fuller, S.D. (2003). Structural organization of authentic, mature HIV-1 virions and cores. EMBO J *22*, 1707-1715.**

**Brown, K.E. (2010). The expanding range of parvoviruses which infect humans. Rev Med Virol *20*, 231-244.**

**Bubeck, D., Filman, D.J., Cheng, N., Steven, A.C., Hogle, J.M., and Belnap, D.M. (2005). The structure of the poliovirus 135S cell entry intermediate at 10-angstrom resolution reveals the location of an externalized polypeptide that binds to membranes. J Virol *79*, 7745-7755.**

**Casjens, S. (1997). Principles of virion structure, function and assembly. In Structural biology of viruses, W. Chiu, R.M. Burnett, and R. Garcea, eds. (New York, Oxford University Press), pp. 3-37.**

**Caspar, D.L., and Klug, A. (1962). Physical principles in the construction of regular viruses. Cold Spring Harb Symp Quant Biol *27*, 1-24.**

**Castano-Diez, D., Al-Amoudi, A., Glynn, A.M., Seybert, A., and Frangakis, A.S. (2007). Fiducial-less alignment of cryo-sections. J Struct Biol *159*, 413-423.**

**Caston, J.R., Trus, B.L., Booy, F.P., Wickner, R.B., Wall, J.S., and Steven, A.C. (1997). Structure of L-A virus: a specialized compartment for the transcription and replication of double-stranded RNA. J Cell Biol *138*, 975-985.**

**Chan, L.G., Parashar, U.D., Lye, M.S., Ong, F.G., Zaki, S.R., Alexander, J.P., Ho, K.K., Han, L.L., Pallansch, M.A., Suleiman, A.B., *et al.* (2000). Deaths of children during an outbreak of hand, foot, and mouth disease in sarawak, malaysia: clinical and pathological characteristics of the disease. For the Outbreak Study Group. Clin Infect Dis *31*, 678-683.**

**Chandrasekar, V., and Johnson, J.E. (1998). The structure of tobacco ringspot virus: a link in the evolution of icosahedral capsids in the picornavirus superfamily. Structure *6*, 157-171.**

**Chandrasekar, V., Munshi, S., and Johnson, J.E. (1997). Crystallization and preliminary X-ray analysis of tobacco ringspot virus. Acta Crystallogr D Biol Crystallogr *53*, 125-128.**

**Chang, K.H., Auvinen, P., Hyypiä, T., and Stanway, G. (1989). The nucleotide sequence of coxsackievirus A9; implications for receptor binding and enterovirus classification. J Gen Virol *70 ( Pt 12)*, 3269-3280.**

**Chang, L.Y., Huang, L.M., Gau, S.S., Wu, Y.Y., Hsia, S.H., Fan, T.Y., Lin, K.L., Huang, Y.C., Lu, C.Y., and Lin, T.Y. (2007). Neurodevelopment and cognition in children after enterovirus 71 infection. N Engl J Med *356*, 1226-1234.**

**Chen, J.Z., Settembre, E.C., Aoki, S.T., Zhang, X., Bellamy, A.R., Dormitzer, P.R., Harrison, S.C., and Grigorieff, N. (2009). Molecular interactions in rotavirus assembly and uncoating seen by high-resolution cryo-EM. Proc Natl Acad Sci U S A *106*, 10644-10648.**

**Chumakov, M., Voroshilova, M., Shindarov, L., Lavrova, I., Gracheva, L., Koroleva, G., Vasilenko, S., Brodvarova, I., Nikolova, M., Gyurova, S., *et al.* (1979). Enterovirus 71 isolated from cases of epidemic poliomyelitis-like disease in Bulgaria. Arch Virol *60*, 329-340.**

**Chung, Y.C., Ho, M.S., Wu, J.C., Chen, W.J., Huang, J.H., Chou, S.T., and Hu, Y.C. (2008). Immunization with virus-like particles of enterovirus 71 elicits potent immune responses and protects mice against lethal challenge. Vaccine *26*, 1855-1862.**

**Collinge, D.B., Jørgensen, H.J., Lund, O.S., and Lyngkjaer, M.F. (2010). Engineering pathogen resistance in crop plants: current trends and future prospects. Annu Rev Phytopathol *48*, 269-291.**

**Convery, M.A., Rowsell, S., Stonehouse, N.J., Ellington, A.D., Hirao, I., Murray, J.B., Peabody, D.S., Phillips, S.E., and Stockley, P.G. (1998). Crystal structure of an RNA aptamer-protein complex at 2.8 A resolution. Nat Struct Biol *5*, 133-139.**

**Coyne, C.B., and Bergelson, J.M. (2006). Virus-induced Abl and Fyn kinase signals permit coxsackievirus entry through epithelial tight junctions. Cell *124*, 119-131.**

**Crowther, R.A. (1971a). Procedures for three-dimensional reconstruction of spherical viruses by Fourier synthesis**

**from electron micrographs. Philos Trans R Soc Lond B Biol Sci *261*, 221-230.**

**Crowther, R.A. (1971b). Three-dimensional reconstruction and the architecture of spherical viruses. Endeavour *30*, 124-129.**

**Crowther, R.A., Amos, L.A., Finch, J.T., De Rosier, D.J., and Klug, A. (1970). Three dimensional reconstructions of spherical viruses by fourier synthesis from electron micrographs. Nature *226*, 421-425.**

**Daberkow, I., Hermann, K.-H., Liu, L., and Rau, W.D. (1991). Performance of electron image converters with YAG single crystal screen and CCD sensor. Ultramicroscopy *38*, 215-223.**

**Danthi, P., Tosteson, M., Li, Q.H., and Chow, M. (2003). Genome delivery and ion channel properties are altered in VP4 mutants of poliovirus. J Virol *77*, 5266-5274.**

**De Cock, K.M., and De Lay, P. (2008). HIV/AIDS estimates and the quest for universal access. Lancet *371*, 2068-2070.**

**Dedryver, C.A., Le Ralec, A., and Fabre, F. (2010). The conflicting relationships between aphids and men: a review of aphid damage and control strategies. C R Biol *333*, 539-553.**

**Dehesa-Violante, M., and Nunez-Nateras, R. (2007). Epidemiology of hepatitis virus B and C. Arch Med Res *38*, 606-611.**

**Desnues, C., and Raoult, D. (2010). Inside the lifestyle of the virophage. Intervirology *53*, 293-303.**

**DeTulleo, L., and Kirchhausen, T. (1998). The clathrin endocytic pathway in viral infection. EMBO J *17*, 4585-4593.**

**Diener, T.O., and Schneider, I.R. (1966). The two components of tobacco ringspot virus nucleic acid: origin and properties. Virology *29*, 100-105.**

**Downing, K.H., and Hendrickson, F.M. (1999). Performance of a 2k CCD camera designed for electron crystallography at 400 kV. Ultramicroscopy *75*, 215-233.**

**Dubochet, J., Adrian, M., Chang, J.J., Homo, J.C., Lepault, J., McDowall, A.W., and Schultz, P. (1988). Cryo-electron microscopy of vitrified specimens. Q Rev Biophys *21*, 129-228.**

**Dykeman, E.C., Stockley, P.G., and Twarock, R. (2010). Dynamic allostery controls coat protein conformer switching during MS2 phage assembly. J Mol Biol *395*, 916-923.**

**Ehrenfeld, E., Modlin, J., and Chumakov, K. (2009). Future of polio vaccines. Expert Rev Vaccines *8*, 899-905.**

**Erickson, H.P., and Klug, A. (1971). Measurement and compensation of defocusing and aberrations by Fourier processing of electron micrographs. Phil Trans R Soc Lond B *261*, 105-118.**

**Faruqi, A.R. (2009). Principles and prospects of direct high resolution electron image acquisition with CMOS detectors at low energies. J Phys: Condens Matter *21*.**

**Faruqi, A.R., and Andrews, H.N. (1997). Cooled CCD camera with tapered fibre optics for electron microscopy. Nuclear Instruments and Methods in Physics Research A *392*, 233-236.**

**Faruqi, A.R., and Henderson, R. (2007). Electronic detectors for electron microscopy. Curr Opin Struct Biol *17*, 549-555.**

**Faruqi, A.R., and Subramaniam, S. (2000). CCD detectors in high-resolution biological electron microscopy. Q Rev Biophys *33*, 1-27.**

**Faruqi, A.R., and Tyrell, G.C. (1999). Evaluation of gadolinium oxy-sulphide (P43) phosphor used in CCD detectors for electron microscopy. Ultramicroscopy *76*, 69-75.**

**Fernandez, J.J., Luque, D., Caston, J.R., and Carrascosa, J.L. (2008). Sharpening high resolution information in single particle electron cryomicroscopy. J Struct Biol *164*, 170-175.**

**Forster, R.L., and Morris-Krsinich, B.A. (1985). Synthesis and processing of the translation products of tobacco ringspot virus in rabbit reticulocyte lysates. Virology *144*, 516-519.**

**Fox, J.M., Wang, G., Speir, J.A., Olson, N.H., Johnson, J.E., Baker, T.S., and Young, M.J. (1998). Comparison of the native CCMV virion with in vitro assembled CCMV virions by cryoelectron microscopy and image reconstruction. Virology *244*, 212-218.**

**Fricks, C.E., and Hogle, J.M. (1990). Cell-induced conformational change in poliovirus: externalization of the amino terminus of VP1 is responsible for liposome binding. J Virol *64*, 1934-1945.**

**Fry, E., Acharya, R., and Stuart, D. (1993). Methods used in the structure determination of foot-and-mouth disease virus. Acta Crystallogr A *49 ( Pt 1)*, 45-55.**

**Fry, E.E., Lea, S.M., Jackson, T., Newman, J.W., Ellard, F.M., Blakemore, W.E., Abu-Ghazaleh, R., Samuel, A., King, A.M., and Stuart, D.I. (1999). The structure and function of a foot-and-mouth disease virus-oligosaccharide receptor complex. EMBO J *18*, 543-554.**

**Fuller, S.D., Butcher, S.J., Cheng, R.H., and Baker, T.S. (1996). Three-dimensional reconstruction of icosahedral particles--the uncommon line. J Struct Biol *116*, 48-55.**

**Golmohammadi, R., Valegård, K., Fridborg, K., and Liljas, L. (1993). The refined structure of bacteriophage MS2 at 2.8 A resolution. J Mol Biol *234*, 620-639.**

**Goncalves, R.B., Mendes, Y.S., Soares, M.R., Katpally, U., Smith, T.J., Silva, J.L., and Oliveira, A.C. (2007). VP4 protein from human rhinovirus 14 is released by pressure and locked in the capsid by the antiviral compound WIN. J Mol Biol *366*, 295-306.**

**Grist, N.R. (1962). Type A7 Coxsackie (type 4 poliomyelitis) virus infection in Scotland. J Hyg (Lond) *60*, 323-332.**

**Grist, N.R. (1969). Coxsackie A7 virus and poliomyelitis in vaccines. Lancet *1*, 575.**

**Grist, N.R., and Bell, E.J. (1984). Paralytic poliomyelitis and nonpolio enteroviruses: studies in Scotland. Rev Infect Dis *6 Suppl 2*, S385-386.**

**Grubman, M.J., Moraes, M.P., Diaz-San Segundo, F., Pena, L., and de los Santos, T. (2008). Evading the host immune response: how foot-and-mouth disease virus has become an effective pathogen. FEMS Immunol Med Microbiol *53*, 8-17.**

**Grunert, H.P., Wolf, K.U., Langner, K.D., Sawitzky, D., Habermehl, K.O., and Zeichhardt, H. (1997). Internalization of human rhinovirus 14 into HeLa and ICAM-1-transfected BHK cells. Med Microbiol Immunol *186*, 1-9.**

**Grünewald, K., Medalia, O., Gross, A., Steven, A.C., and Baumeister, W. (2003). Prospects of electron cryotomography to**

**visualize macromolecular complexes inside cellular compartments: implications of crowding. Biophys Chem *100*, 577-591.**

**Habel, K., and Loomis, L.N. (1957). Coxsackie A7 virus and the Russian poliovirus Type 4. Proc Soc Exp Biol Med *95*, 597-605.**

**Hadfield, A.T., Oliveira, M.A., Kim, K.H., Minor, I., Kremer, M.J., Heinz, B.A., Shepard, D., Pevear, D.C., Rueckert, R.R., and Rossmann, M.G. (1995). Structural studies on human rhinovirus 14 drug-resistant compensation mutants. J Mol Biol *253*, 61-73.**

**Hansbro, N.G., Horvat, J.C., Wark, P.A., and Hansbro, P.M. (2008). Understanding the mechanisms of viral induced asthma: new therapeutic directions. Pharmacol Ther *117*, 313-353.**

**Harrison, B.D., Robertson, W.M., and Taylor, C.E. (1974). Specificity of retention and transmission of viruses by nematodes. J Nematol *6*, 155-164.**

**Harrison, S.C., Olson, A.J., Schutt, C.E., Winkler, F.K., and Bricogne, G. (1978). Tomato bushy stunt virus at 2.9 A resolution. Nature *276*, 368-373.**

**Harvala, H., Kalimo, H., Stanway, G., and Hyypiä, T. (2003). Pathogenesis of coxsackievirus A9 in mice: role of the viral arginine-glycine-aspartic acid motif. J Gen Virol *84*, 2375-2379.**

**Hayden, F.G. (2004). Rhinovirus and the lower respiratory tract. Rev Med Virol *14*, 17-31.**

**Hayward, S.B., and Glaeser, R.M. (1979). Radiation damage of purple membrane at low temperature. Ultramicroscopy *04*, 201-210.**

**He, Y., Bowman, V.D., Mueller, S., Bator, C.M., Bella, J., Peng, X., Baker, T.S., Wimmer, E., Kuhn, R.J., and Rossmann, M.G. (2000). Interaction of the poliovirus receptor with poliovirus. Proc Natl Acad Sci U S A *97*, 79-84.**

**He, Y., Chipman, P.R., Howitt, J., Bator, C.M., Whitt, M.A., Baker, T.S., Kuhn, R.J., Anderson, C.W., Freimuth, P., and Rossmann, M.G. (2001). Interaction of coxsackievirus B3 with the full length coxsackievirus-adenovirus receptor. Nat Struct Biol *8*, 874-878.**

**He, Y., Mueller, S., Chipman, P.R., Bator, C.M., Peng, X., Bowman, V.D., Mukhopadhyay, S., Wimmer, E., Kuhn, R.J., and Rossmann, M.G. (2003). Complexes of poliovirus serotypes with their common cellular receptor, CD155. J Virol *77*, 4827-4835.**

**Hendry, E., Hatanaka, H., Fry, E., Smyth, M., Tate, J., Stanway, G., Santti, J., Maaronen, M., Hyypiä, T., and Stuart, D. (1999). The crystal structure of coxsackievirus A9: new insights into the uncoating mechanisms of enteroviruses. Structure *7*, 1527-1538.**

**Hewat, E.A., and Blaas, D. (2004). Cryoelectron microscopy analysis of the structural changes associated with human rhinovirus type 14 uncoating. J Virol *78*, 2935-2942.**

**Ho, M., Chen, E.R., Hsu, K.H., Twu, S.J., Chen, K.T., Tsai, S.F., Wang, J.R., and Shih, S.R. (1999). An epidemic of enterovirus 71 infection in Taiwan. Taiwan Enterovirus Epidemic Working Group. N Engl J Med *341*, 929-935.**

**Hober, D., and Sane, F. (2010). Enteroviral pathogenesis of type 1 diabetes. Discov Med *10*, 151-160.**

**Hogle, J.M. (2002). Poliovirus cell entry: common structural themes in viral cell**

**entry pathways. Annu Rev Microbiol *56*, 677-702.**

**Hogle, J.M., Chow, M., and Filman, D.J. (1985). Three-dimensional structure of poliovirus at 2.9 A resolution. Science *229*, 1358-1365.**

**Hoover-Litty, H., and Greve, J.M. (1993). Formation of rhinovirus-soluble ICAM-1 complexes and conformational changes in the virion. J Virol *67*, 390-397.**

**Horn, W.T., Tars, K., Grahn, E., Helgstrand, C., Baron, A.J., Lago, H., Adams, C.J., Peabody, D.S., Phillips, S.E., Stonehouse, N.J., *et al.* (2006). Structural basis of RNA binding discrimination between bacteriophages Qbeta and MS2. Structure *14*, 487-495.**

**Hughes, P.J., Horsnell, C., Hyypiä, T., and Stanway, G. (1995). The coxsackievirus A9 RGD motif is not essential for virus viability. J Virol *69*, 8035-8040.**

**Hyypiä, T., Horsnell, C., Maaronen, M., Khan, M., Kalkkinen, N., Auvinen, P., Kinnunen, L., and Stanway, G. (1992). A distinct picornavirus group identified by sequence analysis. Proc Natl Acad Sci U S A *89*, 8847-8851.**

**Jaidane, H., Sauter, P., Sane, F., Goffard, A., Gharbi, J., and Hober, D. (2010). Enteroviruses and type 1 diabetes: towards a better understanding of the relationship. Rev Med Virol *20*, 265-280.**

**Ji, Y., Marinescu, D.C., Zhang, W., Zhang, X., Yan, X., and Baker, T.S. (2006). A model-based parallel origin and orientation refinement algorithm for cryoTEM and its application to the study of virus structures. J Struct Biol *154*, 1-19.**

**Jobling, S.A., and Wood, K.R. (1985). Translation of Tobacco Ringspot Virus RNA in Reticulocyte Lysate: Proteolytic Processing of the Primary Translation Products. J Gen Virol *66*, 2589-2596.**

**Johnson, J.E. (1996). Functional implications of protein-protein interactions in icosahedral viruses. Proc Natl Acad Sci U S A *93*, 27-33.**

**Johnston, S.L. (2005). Overview of virus-induced airway disease. Proc Am Thorac Soc *2*, 150-156.**

**Joki-Korpela, P., and Hyypiä, T. (2001). Parechoviruses, a novel group of human picornaviruses. Ann Med *33*, 466-471.**

**Joki-Korpela, P., Marjomäki, V., Krogerus, C., Heino, J., and Hyypiä, T. (2001). Entry of human parechovirus 1. J Virol *75*, 1958-1967.**

**Jones, A.T. (2000). Black currant reversion disease--the probable causal agent, eriophyid mite vectors, epidemiology and prospects for control. Virus Res *71*, 71-84.**

**Jones, A.T., and McGavin, W.J. (2002). Improved PCR Detection of *Blackcurrant reversion virus* in *Ribes* and Further Evidence that It Is the Causal Agent of Reversion Disease. Plant Disease *86*, 1333-1338.**

**Katpally, U., and Smith, T.J. (2007). Pocket factors are unlikely to play a major role in the life cycle of human rhinovirus. J Virol *81*, 6307-6315.**

**Kelley, L.A., and Sternberg, M.J. (2009). Protein structure prediction on the Web: a case study using the Phyre server. Nat Protoc *4*, 363-371.**

**Kew, O., Morris-Glasgow, V., Landaverde, M., Burns, C., Shaw, J., Garib, Z., Andre, J., Blackman, E., Freeman, C.J., Jorba, J., *et al.* (2002). Outbreak of poliomyelitis in Hispaniola**

**associated with circulating type 1 vaccine-derived poliovirus. Science *296*, 356-359.**

**Khan, A.G., Pickl-Herk, A., Gajdzik, L., Marlovits, T.C., Fuchs, R., and Blaas, D. (2010). Human rhinovirus 14 enters rhabdomyosarcoma cells expressing icam-1 by a clathrin-, caveolin-, and flotillin-independent pathway. J Virol *84*, 3984-3992.**

**Kivioja, T., Ravantti, J., Verkhovsky, A., Ukkonen, E., and Bamford, D. (2000). Local average intensity-based method for identifying spherical particles in electron micrographs. J Struct Biol *131*, 126-134.**

**Klein, J. (2009). Understanding the molecular epidemiology of foot-and-mouth-disease virus. Infect Genet Evol *9*, 153-161.**

**Knapek, E., and Dubochet, J. (1980). Beam damage to organic material is considerably reduced in cryo-electron microscopy. J Mol Biol *141*, 147-161.**

**Kobayashi, A., Fujigaya, T., Itoh, M., Taguchi, T., and Takano, H. (2009). Technical note: a tool for determining rotational tilt axis with or without fiducial markers. Ultramicroscopy *110*, 1-6.**

**Kremer, J.R., Mastronarde, D.N., and McIntosh, J.R. (1996). Computer visualization of three-dimensional image data using IMOD. J Struct Biol *116*, 71-76.**

**Krishnaswamy, S., and Rossmann, M.G. (1990). Structural refinement and analysis of Mengo virus. J Mol Biol *211*, 803-844.**

**Lasker, K., Topf, M., Sali, A., and Wolfson, H.J. (2009). Inferential optimization for simultaneous fitting of multiple components into a CryoEM map of their assembly. J Mol Biol *388*, 180-194.**

**Latvala, S., Susi, P., Kalkkinen, N., and Lehto, K. (1998). Characterization of the coat protein gene of mite-transmitted blackcurrant reversion associated nepovirus. Virus Res *53*, 1-11.**

**Lee, M.S., and Chang, L.Y. (2010). Development of enterovirus 71 vaccines. Expert Rev Vaccines *9*, 149-156.**

**Lemmetty, A., Latvala, S., Jones, A.T., Susi, P., McGavin, W.J., and Lehto, K. (1997). Purification and properties of a new virus from black currant, its affinities with nepoviruses, and its close association with black currant reversion disease. Phytopathology *87*, 404-413.**

**Lemmetty, A., and Lehto, K. (1999). Successful back-inoculation confirms the role of black currant reversion associated virus as the causal agent of reversion disease. Eur J Plant Pathol *105*, 297-301.**

**Levy, H.C., Bostina, M., Filman, D.J., and Hogle, J.M. (2010). Catching a virus in the act of RNA release: a novel poliovirus uncoating intermediate characterized by cryo-electron microscopy. J Virol *84*, 4426-4441.**

**Liddington, R.C., Yan, Y., Moulai, J., Sahli, R., Benjamin, T.L., and Harrison, S.C. (1991). Structure of simian virus 40 at 3.8-A resolution. Nature *354*, 278-284.**

**Lin, J.Y., Chen, T.C., Weng, K.F., Chang, S.C., Chen, L.L., and Shih, S.R. (2009). Viral and host proteins involved in picornavirus life cycle. J Biomed Sci *16*, 103.**

**Liu, H., Jin, L., Koh, S.B., Atanasov, I., Schein, S., Wu, L., and Zhou, Z.H. (2010). Atomic structure of human adenovirus by cryo-EM reveals**

**interactions among protein networks. Science *329*, 1038-1043.**

**Loebenstein, G. (2009). Local lesions and induced resistance. Adv Virus Res *75*, 73-117.**

**Ludtke, S.J., Baldwin, P.R., and Chiu, W. (1999). EMAN: semiautomated software for high-resolution single-particle reconstructions. J Struct Biol *128*, 82-97.**

**Macfarlane, S.A. (2010). Tobraviruses--plant pathogens and tools for biotechnology. Mol Plant Pathol *11*, 577-583.**

**Mardones, F., Perez, A., Sanchez, J., Alkhamis, M., and Carpenter, T. (2010). Parameterization of the duration of infection stages of serotype O foot-and-mouth disease virus: an analytical review and meta-analysis with application to simulation models. Vet Res *41*, 45.**

**Marinescu, D.C., and Ji, Y. (2003). A computational framework for the 3D structure determination of viruses with unknown symmetry. Journal of Parallel and Distributed Computing *63*, 738-758.**

**Marsh, M., and Helenius, A. (2006). Virus entry: open sesame. Cell *124*, 729-740.**

**Masich, S., Ostberg, T., Norlen, L., Shupliakov, O., and Daneholt, B. (2006). A procedure to deposit fiducial markers on vitreous cryo-sections for cellular tomography. J Struct Biol *156*, 461-468.**

**Mastronarde, D.N. (2005). Automated electron microscope tomography using robust prediction of specimen movements. J Struct Biol *152*, 36-51.**

**Mayo, M.A., Murant, A.F., Harrison, B.D., and Goold, R.A. (1974). Two protein and two RNA species in particles of strawberry latent ringspot virus. J Gen Virol *24*, 29-37.**

**McMullan, G., Faruqi, A.R., Henderson, R., Guerrini, N., Turchetta, R., Jacobs, A., and van Hoften, G. (2009). Experimental observation of the improvement in MTF from backthinning a CMOS direct electron detector. Ultramicroscopy *109*, 1144-1147.**

**Mendelsohn, C.L., Wimmer, E., and Racaniello, V.R. (1989). Cellular receptor for poliovirus: molecular cloning, nucleotide sequence, and expression of a new member of the immunoglobulin superfamily. Cell *56*, 855-865.**

**Mercer, J., Schelhaas, M., and Helenius, A. (2010). Virus entry by endocytosis. Annu Rev Biochem *79*, 803-833.**

**Miller, S.T., Hogle, J.M., and Filman, D.J. (2001). Ab initio phasing of high-symmetry macromolecular complexes: successful phasing of authentic poliovirus data to 3.0 A resolution. J Mol Biol *307*, 499-512.**

**Mindell, J.A., and Grigorieff, N. (2003). Accurate determination of local defocus and specimen tilt in electron microscopy. J Struct Biol *142*, 334-347.**

**Minor, P.D. (1996). Poliovirus biology. Structure *4*, 775-778.**

**Morton, V.L., Dykeman, E.C., Stonehouse, N.J., Ashcroft, A.E., Twarock, R., and Stockley, P.G. (2010). The impact of viral RNA on assembly pathway selection. J Mol Biol *401*, 298-308.**

**Muckelbauer, J.K., Kremer, M., Minor, I., Tong, L., Zlotnick, A., Johnson, J.E., and Rossmann, M.G. (1995). Structure determination of coxsackievirus B3 to 3.5**

**A resolution. Acta Crystallogr D Biol Crystallogr *51*, 871-887.**

**Murant, A.F., Taylor, M., Duncan, G.H., and Raschke, J.H. (1981). Improved Estimates of Molecular Weight of Plant Virus RNA by Agarose Gel Electrophoresis and Electron Microscopy after Denaturation with Glyoxal. J Gen Virol *53*, 321-332.**

**Namba, K., and Stubbs, G. (1986). Structure of tobacco mosaic virus at 3.6 A resolution: implications for assembly. Science *231*, 1401-1406.**

**Nandhagopal, N., Simpson, A.A., Gurnon, J.R., Yan, X., Baker, T.S., Graves, M.V., Van Etten, J.L., and Rossmann, M.G. (2002). The structure and evolution of the major capsid protein of a large, lipid-containing DNA virus. Proc Natl Acad Sci U S A *99*, 14758-14763.**

**Nemerow, G.R. (2000). Cell receptors involved in adenovirus entry. Virology *274*, 1-4.**

**Nishimura, Y., Shimojima, M., Tano, Y., Miyamura, T., Wakita, T., and Shimizu, H. (2009). Human P-selectin glycoprotein ligand-1 is a functional receptor for enterovirus 71. Nat Med *15*, 794-797.**

**Nurani, G., Lindqvist, B., and Casasnovas, J.M. (2003). Receptor priming of major group human rhinoviruses for uncoating and entry at mild low-pH environments. J Virol *77*, 11985-11991.**

**Oberste, M.S., Penaranda, S., Maher, K., and Pallansch, M.A. (2004). Complete genome sequences of all members of the species Human enterovirus A. J Gen Virol *85*, 1597-1607.**

**Oliveira, A.C., Ishimaru, D., Goncalves, R.B., Smith, T.J., Mason, P., Sa-Carvalho, D., and Silva, J.L. (1999). Low temperature and pressure stability of picornaviruses: implications for virus uncoating. Biophys J *76*, 1270-1279.**

**Orlova, E.V., and Saibil, H.R. (2004). Structure determination of macromolecular assemblies by single-particle analysis of cryo-electron micrographs. Curr Opin Struct Biol *14*, 584-590.**

**Parashar, U.D., Burton, A., Lanata, C., Boschi-Pinto, C., Shibuya, K., Steele, D., Birmingham, M., and Glass, R.I. (2009). Global mortality associated with rotavirus disease among children in 2004. J Infect Dis *200 Suppl 1*, S9-S15.**

**Pelkmans, L., and Helenius, A. (2003). Insider information: what viruses tell us about endocytosis. Curr Opin Cell Biol *15*, 414-422.**

**Penczek, P., Marko, M., Buttle, K., and Frank, J. (1995). Double-tilt electron tomography. Ultramicroscopy *60*, 393-410.**

**Perring, T.M., Gruenhagen, N.M., and Farrar, C.A. (1999). Management of plant viral diseases through chemical control of insect vectors. Annu Rev Entomol *44*, 457-481.**

**Pettersen, E.F., Goddard, T.D., Huang, C.C., Couch, G.S., Greenblatt, D.M., Meng, E.C., and Ferrin, T.E. (2004). UCSF Chimera--a visualization system for exploratory research and analysis. J Comput Chem *25*, 1605-1612.**

**Pietiäinen, V., Marjomäki, V., Upla, P., Pelkmans, L., Helenius, A., and Hyypiä, T. (2004). Echovirus 1 endocytosis into caveosomes requires lipid rafts, dynamin II, and signaling events. Mol Biol Cell *15*, 4911-4925.**

**Pulli, T., Koivunen, E., and Hyypiä, T. (1997). Cell-surface interactions of echovirus 22. J Biol Chem *272*, 21176-21180.**

**Purkayastha, A., and Dasgupta, I. (2009). Virus-induced gene silencing: a versatile tool for discovery of gene functions in plants. Plant Physiol Biochem *47*, 967-976.**

**Racaniello, V.R. (2006). One hundred years of poliovirus pathogenesis. Virology *344*, 9-16.**

**Rayment, I., Baker, T.S., Caspar, D.L., and Murakami, W.T. (1982). Polyoma virus capsid structure at 22.5 A resolution. Nature *295*, 110-115.**

**Reddy, D.V., Sudarshana, M.R., Fuchs, M., Rao, N.C., and Thottappilly, G. (2009). Genetically engineered virus-resistant plants in developing countries: current status and future prospects. Adv Virus Res *75*, 185-220.**

**Richter, F.A., Rhodes, A.J., Macpherson, L.W., and Labzoffsky, N.A. (1971). A possible new enterovirus serotype isolated in Ontario. Arch Gesamte Virusforsch *35*, 218-222.**

**Robbins, F.C., and de Quadros, C.A. (1997). Certification of the eradication of indigenous transmission of wild poliovirus in the Americas. J Infect Dis *175 Suppl 1*, S281-285.**

**Roberts, M.M., White, J.L., Grutter, M.G., and Burnett, R.M. (1986). Three-dimensional structure of the adenovirus major coat protein hexon. Science *232*, 1148-1151.**

**Roivainen, M., Piirainen, L., Hovi, T., Virtanen, I., Riikonen, T., Heino, J., and Hyypiä, T. (1994). Entry of coxsackievirus A9 into host cells: specific interactions with alpha v beta 3 integrin, the vitronectin receptor. Virology *203*, 357-365.**

**Rolfsson, O., Toropova, K., Ranson, N.A., and Stockley, P.G. (2010). Mutually-induced conformational switching of RNA and coat protein underpins efficient assembly of a viral capsid. J Mol Biol *401*, 309-322.**

**Roossinck, M.J. (2010). Lifestyles of plant viruses. Philos Trans R Soc Lond B Biol Sci *365*, 1899-1905.**

**Rosenthal, P.B., and Henderson, R. (2003). Optimal determination of particle orientation, absolute hand, and contrast loss in single-particle electron cryomicroscopy. J Mol Biol *333*, 721-745.**

**Rossmann, M.G. (1994). Viral cell recognition and entry. Protein Sci *3*, 1712-1725.**

**Rossmann, M.G., Arnold, E., Erickson, J.W., Frankenberger, E.A., Griffith, J.P., Hecht, H.J., Johnson, J.E., Kamer, G., Luo, M., Mosser, A.G., *et al.* (1985). Structure of a human common cold virus and functional relationship to other picornaviruses. Nature *317*, 145-153.**

**Roth, B.M., Pruss, G.J., and Vance, V.B. (2004). Plant viral suppressors of RNA silencing. Virus Res *102*, 97-108.**

**Roy, A., Kucukural, A., and Zhang, Y. (2010). I-TASSER: a unified platform for automated protein structure and function prediction. Nat Protoc *5*, 725-738.**

**Ryan, M.D., and Flint, M. (1997). Virus-encoded proteinases of the picornavirus super-group. J Gen Virol *78 ( Pt 4)*, 699-723.**

**Saban, S.D., Silvestry, M., Nemerow, G.R., and Stewart, P.L. (2006). Visualization of alpha-helices in a 6-**

**angstrom resolution cryoelectron microscopy structure of adenovirus allows refinement of capsid protein assignments. J Virol *80*, 12049-12059.**

**Sabin, A.B., Hennessen, W.A., and Winsser, J. (1954). Studies on variants of poliomyelitis virus. I. Experimental segregation and properties of avirulent variants of three immunologic types. J Exp Med *99*, 551-576.**

**Salk, J.E., Bazeley, P.L., Bennett, B.L., Krech, U., Lewis, L.J., Ward, E.N., and Youngner, J.S. (1954a). Studies in human subjects on active immunization against poliomyelitis. II. A practical means for inducing and maintaining antibody formation. Am J Public Health Nations Health *44*, 994-1009.**

**Salk, J.E., Krech, U., Youngner, J.S., Bennett, B.L., Lewis, L.J., and Bazeley, P.L. (1954b). Formaldehyde treatment and safety testing of experimental poliomyelitis vaccines. Am J Public Health Nations Health *44*, 563-570.**

**Schmidt, N.J., Lennette, E.H., and Ho, H.H. (1974). An apparently new enterovirus isolated from patients with disease of the central nervous system. J Infect Dis *129*, 304-309.**

**Schröder, R.R. (1992). Zero-loss energy-filtered imaging of frozen-hydrated proteins: model calculations and implications for future developments. J Microsc *166*, 389-400.**

**Schröder, R.R., Hofmann, W., and Ménétret, J.-F. (1990). Zero-Loss Energy Filtering as Improved Imaging Mode in Cryoelectronmicroscopy of Frozen-Hydrated Specimens. Journal of Structural Biology *105*, 28-34.**

**Shaw, J.G. (1999). Tobacco mosaic virus and the study of early events in virus infections. Philos Trans R Soc Lond B Biol Sci *354*, 603-611.**

**Shepherd, C.M., Borelli, I.A., Lander, G., Natarajan, P., Siddavanahalli, V., Bajaj, C., Johnson, J.E., Brooks, C.L., 3rd, and Reddy, V.S. (2006). VIPERdb: a relational database for structural virology. Nucleic Acids Res *34*, D386-389.**

**Singh, R.P., Valkonen, J.P., Gray, S.M., Boonham, N., Jones, R.A., Kerlan, C., and Schubert, J. (2008). Discussion paper: The naming of Potato virus Y strains infecting potato. Arch Virol *153*, 1-13.**

**Singh, S., Rothnagel, R., Prasad, B.V., and Buckley, B. (1995). Expression of tobacco ringspot virus capsid protein and satellite RNA in insect cells and three-dimensional structure of tobacco ringspot virus-like particles. Virology *213*, 472-481.**

**Smith, A.E., and Helenius, A. (2004). How viruses enter animal cells. Science *304*, 237-242.**

**Smith, T.J., Kremer, M.J., Luo, M., Vriend, G., Arnold, E., Kamer, G., Rossmann, M.G., McKinlay, M.A., Diana, G.D., and Otto, M.J. (1986). The site of attachment in human rhinovirus 14 for antiviral agents that inhibit uncoating. Science *233*, 1286-1293.**

**Stanway, G., Joki-Korpela, P., and Hyypiä, T. (2000). Human parechoviruses--biology and clinical significance. Rev Med Virol *10*, 57-69.**

**Stanway, G., Kalkkinen, N., Roivainen, M., Ghazi, F., Khan, M., Smyth, M., Meurman, O., and Hyypiä, T. (1994). Molecular and biological characteristics of echovirus 22, a representative of a new picornavirus group. J Virol *68*, 8232-8238.**

**Steven, A.C., and Aebi, U. (2003). The next ice age: cryo-electron tomography of intact cells. Trends Cell Biol *13*, 107-110.**

**Stockley, P.G., Rolfsson, O., Thompson, G.S., Basnak, G., Francese, S., Stonehouse, N.J., Homans, S.W., and Ashcroft, A.E. (2007). A simple, RNA-mediated allosteric switch controls the pathway to formation of a T=3 viral capsid. J Mol Biol *369*, 541-552.**

**Tauriainen, S., Oikarinen, S., Oikarinen, M., and Hyöty, H. (2010). Enteroviruses in the pathogenesis of type 1 diabetes. Semin Immunopathol.**

**Tee, K.K., Takebe, Y., and Kamarulzaman, A. (2009). Emerging and re-emerging viruses in Malaysia, 1997-2007. Int J Infect Dis *13*, 307-318.**

**Thresh, J.M. (1964). Association between black currant reversion virus and its gall mite vector (Phytoptus Ribis Nal.). Nature *202*, 1085-1087.**

**Tilton, J.C., and Doms, R.W. (2010). Entry inhibitors in the treatment of HIV-1 infection. Antiviral Res *85*, 91-100.**

**Topf, M., Baker, M.L., Marti-Renom, M.A., Chiu, W., and Sali, A. (2006). Refinement of protein structures by iterative comparative modeling and CryoEM density fitting. J Mol Biol *357*, 1655-1668.**

**Topf, M., Lasker, K., Webb, B., Wolfson, H., Chiu, W., and Sali, A. (2008). Protein structure fitting and refinement guided by cryo-EM density. Structure *16*, 295-307.**

**Toropova, K., Basnak, G., Twarock, R., Stockley, P.G., and Ranson, N.A. (2008). The three-dimensional structure of genomic RNA in bacteriophage MS2: implications for assembly. J Mol Biol *375*, 824-836.**

**Toyoshima, C., and Unwin, N. (1988). Contrast transfer for frozen-hydrated specimens: determination from pairs of defocused images. Ultramicroscopy *25*, 279-291.**

**Tuthill, T.J., Bubeck, D., Rowlands, D.J., and Hogle, J.M. (2006). Characterization of early steps in the poliovirus infection process: receptor-decorated liposomes induce conversion of the virus to membrane-anchored entry-intermediate particles. J Virol *80*, 172-180.**

**Twarock, R. (2004). A tiling approach to virus capsid assembly explaining a structural puzzle in virology. J Theor Biol *226*, 477-482.**

**Twarock, R. (2006). Mathematical virology: a novel approach to the structure and assembly of viruses. Philos Transact A Math Phys Eng Sci *364*, 3357-3373.**

**Uncapher, C.R., DeWitt, C.M., and Colonno, R.J. (1991). The major and minor group receptor families contain all but one human rhinovirus serotype. Virology *180*, 814-817.**

**Wade, R.H. (1992). A brief look at imaging and contrast transfer. Ultramicroscopy *46*, 145-156.**

**Valegård, K., Murray, J.B., Stockley, P.G., Stonehouse, N.J., and Liljas, L. (1994). Crystal structure of an RNA bacteriophage coat protein-operator complex. Nature *371*, 623-626.**

**Valegård, K., Murray, J.B., Stonehouse, N.J., van den Worm, S., Stockley, P.G., and Liljas, L. (1997). The three-dimensional structures of two complexes between recombinant MS2 capsids and RNA operator fragments reveal**

**sequence-specific protein-RNA interactions. J Mol Biol *270*, 724-738.**

**Walton, R.P., and Johnston, S.L. (2008). Role of respiratory viral infections in the development of atopic conditions. Curr Opin Allergy Clin Immunol *8*, 150-153.**

**van der Sanden, S., Koopmans, M., Uslu, G., and van der Avoort, H. (2009). Epidemiology of enterovirus 71 in the Netherlands, 1963 to 2008. J Clin Microbiol *47*, 2826-2833.**

**van der Sanden, S., van der Avoort, H., Lemey, P., Uslu, G., and Koopmans, M. (2010). Evolutionary trajectory of the VP1 gene of human enterovirus 71 genogroup B and C viruses. J Gen Virol *91*, 1949-1958.**

**Wang, S., and Gergerich, R.C. (1998). Immunofluorescent Localization of Tobacco Ringspot Nepovirus in the Vector Nematode Xiphinema americanum. Phytopathology *88*, 885-889.**

**Wang, S., Gergerich, R.C., Wickizer, S.L., and Kim, K.S. (2002). Localization of Transmissible and Nontransmissible Viruses in the Vector Nematode Xiphinema americanum. Phytopathology *92*, 646-653.**

**Watanabe, Y., Watanabe, K., Katagiri, S., and Hinuma, Y. (1965). Virus-specific proteins produced in HeLa cells infected with poliovirus: characterization of subunit-like protein. J Biochem *57*, 733-741.**

**Weinacker, A., Chen, A., Agrez, M., Cone, R.I., Nishimura, S., Wayner, E., Pytela, R., and Sheppard, D. (1994). Role of the integrin alpha v beta 6 in cell attachment to fibronectin. Heterologous expression of intact and secreted forms of the receptor. J Biol Chem *269*, 6940-6948.**

**Williams, C.H., Kajander, T., Hyypiä, T., Jackson, T., Sheppard, D., and Stanway, G. (2004). Integrin alpha v beta 6 is an RGD-dependent receptor for coxsackievirus A9. J Virol *78*, 6967-6973.**

**Williamson, J.D., and Grist, N.R. (1965). Studies on the haemagglutinin present in Coxsackie A7 virus-infected suckling mouse tissue. J Gen Microbiol *41*, 283-291.**

**Wommack, K.E., and Colwell, R.R. (2000). Virioplankton: viruses in aquatic ecosystems. Microbiol Mol Biol Rev *64*, 69-114.**

**Wu, C.N., Lin, Y.C., Fann, C., Liao, N.S., Shih, S.R., and Ho, M.S. (2002). Protection against lethal enterovirus 71 infection in newborn mice by passive immunization with subunit VP1 vaccines and inactivated virus. Vaccine *20*, 895-904.**

**Wu, Q., Wang, X., and Ding, S.W. (2010). Viral suppressors of RNA-based viral immunity: host targets. Cell Host Microbe *8*, 12-15.**

**Xiao, C., Bator-Kelly, C.M., Rieder, E., Chipman, P.R., Craig, A., Kuhn, R.J., Wimmer, E., and Rossmann, M.G. (2005a). The crystal structure of coxsackievirus A21 and its interaction with ICAM-1. Structure *13*, 1019-1033.**

**Xiao, C., Chipman, P.R., Battisti, A.J., Bowman, V.D., Renesto, P., Raoult, D., and Rossmann, M.G. (2005b). Cryo-electron microscopy of the giant Mimivirus. J Mol Biol *353*, 493-496.**

**Xie, Q., and Chapman, M.S. (1996). Canine parvovirus capsid structure, analyzed at 2.9 A resolution. J Mol Biol *264*, 497-520.**

**Xiong, J.P., Stehle, T., Zhang, R., Joachimiak, A., Frech, M., Goodman,**

**S.L., and Arnaout, M.A. (2002). Crystal structure of the extracellular segment of integrin alpha Vbeta3 in complex with an Arg-Gly-Asp ligand. Science *296*, 151-155.**

**Yamashita, T., Sakae, K., Tsuzuki, H., Suzuki, Y., Ishikawa, N., Takeda, N., Miyamura, T., and Yamazaki, S. (1998). Complete nucleotide sequence and genetic organization of Aichi virus, a distinct member of the Picornaviridae associated with acute gastroenteritis in humans. J Virol *72*, 8408-8412.**

**Yamayoshi, S., Yamashita, Y., Li, J., Hanagata, N., Minowa, T., Takemura, T., and Koike, S. (2009). Scavenger receptor B2 is a cellular receptor for enterovirus 71. Nat Med *15*, 798-801.**

**Yan, X., Sinkovits, R.S., and Baker, T.S. (2007). AUTO3DEM--an automated and high throughput program for image reconstruction of icosahedral particles. J Struct Biol *157*, 73-82.**

**Yang, B., Chuang, H., and Yang, K.D. (2009). Sialylated glycans as receptor and inhibitor of enterovirus 71 infection to DLD-1 intestinal cells. Virol J *6*, 141.**

**Yu, X., Jin, L., and Zhou, Z.H. (2008). 3.88 A structure of cytoplasmic polyhedrosis virus by cryo-electron microscopy. Nature *453*, 415-419.**

**Zhang, P., Borgnia, M.J., Mooney, P., Shi, D., Pan, M., O'Herron, P., Mao, A., Brogan, D., Milne, J.L., and Subramaniam, S. (2003). Automated image acquisition and processing using a new generation of 4K x 4K CCD cameras for cryo electron microscopic studies of macromolecular assemblies. J Struct Biol *143*, 135-144.**

**Zhang, P., Mueller, S., Morais, M.C., Bator, C.M., Bowman, V.D., Hafenstein, S., Wimmer, E., and Rossmann, M.G. (2008a). Crystal structure of CD155 and electron microscopic studies of its complexes with polioviruses. Proc Natl Acad Sci U S A *105*, 18284-18289.**

**Zhang, X., Jin, L., Fang, Q., Hui, W.H., and Zhou, Z.H. (2010). 3.3 A cryo-EM structure of a nonenveloped virus reveals a priming mechanism for cell entry. Cell *141*, 472-482.**

**Zhang, X., Settembre, E., Xu, C., Dormitzer, P.R., Bellamy, R., Harrison, S.C., and Grigorieff, N. (2008b). Near-atomic resolution using electron cryomicroscopy and single-particle reconstruction. Proc Natl Acad Sci U S A *105*, 1867-1872.**

**Zhang, Y. (2008). I-TASSER server for protein 3D structure prediction. BMC Bioinformatics *9*, 40.**

**Zhang, Y. (2009). I-TASSER: fully automated protein structure prediction in CASP8. Proteins *77 Suppl 9*, 100-113.**

**Zimmermann, H., Eggers, H.J., and Nelsen-Salz, B. (1996). Molecular cloning and sequence determination of the complete genome of the virulent echovirus 9 strain barty. Virus Genes *12*, 149-154.**

**Zimmermann, H., Eggers, H.J., Zimmermann, A., Kraus, W., and Nelsen-Salz, B. (1995). Complete nucleotide sequence and biological properties of an infectious clone of prototype echovirus 9. Virus Res *39*, 311-319.**

**Zlotnick, A., Aldrich, R., Johnson, J.M., Ceres, P., and Young, M.J. (2000). Mechanism of capsid assembly for an icosahedral plant virus. Virology *277*, 450-456.**